PROJECT COMPLETION REPORT

On

"Magnetic nanoparticles decorated biodegradable polyurethanes/MWCNT nanocomposites as shape memory materials"

SPONSORED BY

Department of Science & Technology (DST), New Delhi

Sanction No. *SR/S3/ME/0020/2009-SERC, dated 9th July, 2010*

SUBMITTED BY

Prof. Niranjan Karak (Principal Investigator)

Chemical Sciences Department

TEZPUR UNIVERSITY

Tezpur – 784028, Assam

1. Title of the project: ***"Magnetic nanoparticles decorated biodegradable polyurethanes/MWCNT nanocomposites as shape memory materials"***

2. Principal Investigator: Prof. Niranjan Karak

Co-Investigator: Prof. Ashok Kumar and Dr. Manabendra Mandal

3. Implementing Institution and other collaborating Institutions: Tezpur University

4. Date of commencement: 01/11/2010

5. Planned date of completion: 31/10/2013

6. Actual date of completion: 31/10/2013

7. Objectives as stated in the project proposal:

Main Objective:

The main objective of the present investigation is to develop biodegradable polyurethane/multiwalled carbon nanotube nanocomposites decorated by magnetic (Fe/Fe_3O_4) nanoparticles for shape memory application.

This is associated with the following objectives.

i) Preparation of biodegradable polyurethanes from natural resources like vegetable oils by the pre-polymerization technique.

ii) Functionalization of MWCNT by acid treatment followed by reaction with polyamine/polyol.

iii) Preparation of magnetic nanoparticles decorated MWCNT/polyurethane nanocomposites by mechanical shear force followed by ultrasonication at different dose levels of MWCNT.

iv) Characterization of above magnetic nanoparticles decorated MWCNT/polyurethane nanocomposites by spectroscopic and analytical techniques.

v) Evaluation of performance characteristics of the above nanocomposites as biodegradable shape memory polymeric materials by testing microbial biodegradation, cytotoxicity test, shape recovery and shape fixity tests, tensile strength, magnetic properties, etc.

vi) Optimization of composition and processing parameters to obtain the best shape memory material.

8. Deviation made from original objectives if any, while implementing the project and reasons thereof:

In addition to completion of the stated objectives, a few more objectives are successfully achieved. The results, remaining time as well as facilities tempt us to do so

and accordingly we planned, preceded and got the success. The additional objectives are as follows-

i) To prepare and characterize graphene oxide from graphite by modified Hummers' method.
ii) To prepare and characterize graphene oxide based hyperbranched polyurethane nanocomposite by in-situ polymerization.
iii) To characterize the structural morphology of the prepared nanocomposites by XRD and TEM studies.
iv) To studiy the performance characteristics of the characterized nanocomposites by DSC, TGA, UTM, impact tester, scratch resistance, etc. and evaluate shape memory behavior of the nanocomposites.

9. Experimental work giving full details of experimental set up, methods adopted, data collected supported by necessary table, charts, diagrams & photographs:

The details of experimental works are given in different sub-headings below-

i) <u>Synthesis of *Mesua ferrea* L. seed oil/ castor oil/ sunflower oil based hyperbranched polyurethane elastomers</u>

A three-neck round bottom flask was equipped with a nitrogen gas inlet, a mechanical stirrer and a syringe, for this polymerization reaction. Required amounts of PCL and monoglyceride of the *Mesua ferrea L*. seed oil were taken in the reaction flask in xylene with constant stirring. Then the desired amount of TDI was added drop wise into the reaction mixture at room temperature. The reaction was continued for 3 h at temperature of (70±2) °C to obtain a viscous mass, which is treated as pre-polymer. This pre-polymer was then cooled to room temperature. After that triethanolamine as multifunctional polyol and 1, 4-butandiol as chain extender were added into it. The temperature was then raised again to (110±2) °C and stirred continuously for 2.5 h to complete the reaction as indicated by FTIR spectrum. A part of the viscous product was precipitated in water and then dried in vacuum oven at 50 °C for further analysis and the rest amount was solution cast on different substrates for different testing. The same procedure was followed for the synthesis of polyurethanes taking castor oil directly and monoglyceride of sunflower oil. Pentaerythritol was used as multifunctional polyol in the synthesis of monoglyceride of sunflower oil based polyurethane and reaction of second stage was carried out at 70 °C instead of 110 °C to avoid gel formation. In the castor oil based polyurethane castor oil itself used as a multifunctional polyol. Also different types hyperbranched polyurethanes with different weight percentages of monoglyceride of Mesua *ferrea* L. seed oil and

different weight percentage of pentaerythritol were synthesized in the present investigation.

ii) Surface functionalization of MWCNT

Surface of MWCNT was functionalized by three different methods.

Method 1: MWCNT were dispersed in a mixture of sulfuric acid and nitric acid (3:1 v/v) by ultrasonic vibration in a one-necked round bottom flask equipped with a condenser. The suspension was heated in an oil bath at 70 °C for 90 minutes with magnetic stirring. After that, the resulting suspension was filtered, washed with deionized water and then dried.

Method 2: MWCNT were added in dichloromethane (CH_2Cl_2) medium to a 100 ml flask and the suspension was vibrated ultrasonically for 0.5 h. Then cetyl trimethyl ammonium bromide (CTAB) was added as a phase transfer agent and followed by powdered potassium permanganate was added in small portions during a period of 2 h. 5 mL of acetic acid was also added at the reaction mixture. The mixture was then stirred vigorously for 48 h at room temperature. At the last step, the resulting material was obtained after filtering, treatment of concentric HCl, washing with water and finally dried.

Method 3: MWCNT were dispersed in conc. sulfuric acid by ultrasonic vibration in a one-necked round bottom flask equipped with a condenser. Then potassium permanganate was added in small portions in stirring condition. After that the reaction mixture was stirred at room temperature for 1h followed by 1h heating at 70 °C. After completion of the reaction, the mixture was poured into ice cold water containing small amount of hydrogen peroxide. At the last step, the resulting material was obtained after filtering, treatment of concentric HCl, washing with water and finally dried.

iii) Modification of surface functionalized MWCNT

Required amount of dried acid treated MWCNT (a- MWCNT) were dispersed in DMF by utrasonication followed by the addition of excess $SOCl_2$. Then the reaction mixture was stirred at 70 °C for 12 h to form acid chloride functionalized MWCNT (MWCNT-COCl). After washing several times with anhydrous THF, they were dried in a vacuum oven at 40 °C for 3 h. Finally, the MWCNT-COCl was reacted with TEA at 70 °C under magnetic stirring for 12 h to produce TEA functionalized MWCNT (TEA-f-MWCNT) followed by washing with THF. The obtained solid was dried at 40 °C for 3 h.

iv) Preparation of iron oxide nanoparticles

Fe_3O_4 nanoparticles were prepared by co-precipitation method. Required amount of $FeCl_3.6H_2O$ (2.0 g), $FeCl_2.4H_2O$ (1.225 g) and PEG (1.5 g) used as a surfactant were dissolved in deionized water (50 mL) under the nitrogen atmosphere with vigorous stirring

at room temperature. An aqueous solution of ammonia (30%) was then added slowly into the mixture until it turns black. The black solution was then stirred continuously for 30 min. The resultant magnetic nanoparticles were separated by magnetic decantation and rinsed with deionised water until the nanoparticles were neutral. Finally, the washed Fe_3O_4 nanoparticles were dispersed and stored in ethanol solution.

v) Preparation of iron oxide decorated MWCNT(Fe_3O_4-MWCNT)

An amount of 0.04 g of a-MWCNT was ultrasonically dispersed in 50 mL of distilled water for 30 min. Then, 0.1 g of $FeCl_3.6H_2O$ and 0.06 g of $FeCl_2.4H_2O$ were added to the above dispersed solution and stirred continuously under the N_2 atmosphere for 1 h. An aqueous ammonia solution (30%) was then added drop wise into the mixture until the pH was reached to 11–12. Then, the solution was heated at 80 °C for 1.5 h. The black products were separated by magnetic decantation and washed with distilled water until the pH was reached to 7. Finally, the washed Fe_3O_4-MWCNT was dried at 60 ºC for 24 h under the vacuum.

vi) Preparation of NHBPU/a-MWCNT nanocomposites

The pre-polymer was first prepared from required amount of PCL, monoglyceride of *Mesua ferrea* L. seed oil and TDI at (70 ± 5) ºC for 3h. The pre-polymer was then cooled to room temperature and required amount of butandiol, triethanolamine was added. The required amount of a-MWCNT was dispersed in DMF by sonication for 15 min and purged into the system 1 h before the completion of the reaction. Finally, the NHBPU/a-MWCNT was formed as a solution of 25–30% solid content (w/v) after continuing the reaction for 2 h at 110 ºC. The solution was cast on inert substrates, followed by vacuum degassing and drying at 50 ºC for 24 h for different testing and analyses.

vii) Preparation of NHBPU/TEA-*f*-MWCNT nanocomposites

Hyperbranched polyurethane was prepared as mention above. Briefly, the monoglyceride of *Mesua ferrea* L. seed oil (3.78 mol) and PCL (2.8 mol) were taken in the reaction flask with 30 mL of xylene at constant stirring. TDI (14.76 mol) was slowly injected into the reaction mixture and allowed to react for 3 h at (80 ± 5) °C to obtain the pre-polymer. 1, 4-butanediol (2 mol) and TEA (4.12 mol) were added to the pre-polymer at room temperature. The reaction mixture was heated at (80 ± 5) °C for 2 h. Then required amount of TEA-f-MWCNT dispersed in DMF by sonication for 20 min was injected into the above reaction mixture and continued for another 1 h. The reaction was stopped before gelation. The solution was cast on the inert substrates followed by vacuum degassing and drying at 60 ^{0}C for the different testing. The nanocomposites were denoted as NHBPU,

NHBPUMWCNT0.2, NHBPUMWCNT1 and NHBPUMWCNT2 corresponding to the TEA-f-MWCNT content of 0, 0.2, 1 and 2 wt%, respectively.

viii) Preparation of NHBPU/ Fe_3O_4 nanocomposites

NHBPU/Fe_3O_4 nanocomposites were prepared by ex-situ technique. The required amount of Fe_3O_4 nanoparticles were dispersed in ethanol by sonication for 20 min, subsequently, the dispersion was added drop wise into the polymer solution under vigorous stirring. The mixture was stirred 12 h followed by ultrasonication 30 min for homogeneous distribution of Fe_3O_4 nanoparticles in the polymer matrix. The solution was cast on the inert substrates followed by vacuum degassing and drying at 50 ^{0}C for 24 h for different testing and analyses. The composites denoted as NHBPU, NHBPUMNP2, NHBPUMNP5and NHBPUMNP10 corresponding to the Fe_3O_4 content of 0, 2, 5 and 10 wt%, respectively.

ix) Preparation of NHBPU/ Fe_3O_4 -MWCNT nanocomposites

NHBPU/Fe_3O_4-MWCNT nanocomposites were prepared by in-situ technique as similar to NHBPU/TEA-*f*-MWCNT nanocomposites. Required amount of Fe_3O_4-MWCNT dispersed in DMF by sonication for 15 min. Then this dispersion was injected into the reaction mixture in the 2nd step of polymerization before completion of the reaction and continued the reaction for another 1 h. The reaction was stopped before gelation.

x) Preparation of graphene oxide (GO)

GO was prepared by oxidizing the graphite powder in a mixture of concentrated sulphuric acid and $KMnO_4$ based on a modified Hummers method. Briefly, 2 g of graphite powder was stirred in 35 mL 98% H_2SO_4 on a magnetic stirrer for 2 h. Then 6 g of $KMnO_4$ was gradually added into the above solution while keeping the temperature less than 20 °C. The mixture was then stirred at 35 °C for 4 h in an oil-bath. The resulting solution was diluted by adding 90 mL of water under vigorous stirring for 1 h and a dark brown suspension was obtained. The suspension was further treated by adding 30% H_2O_2 solution drop wise until the colour of the solution became bright yellow. The resulting GO suspension was washed by repeated centrifugation, first with 5% aqueous HCl solution to remove excess of manganese salt and then with water until the pH of the solution became neutral. The purified GO was finally dispersed in water (0.5 mg/mL) and ultrasonically exfoliated in an ultrasonic bath resulted a stable dispersion.

xi) Preparation of NHBPU/ GO nanocomposites

CHBPU/GO nanocomposites were prepared by in-situ technique as similar to NHBPU/TEA-*f*-MWCNT nanocomposites. Required amount of GO dispersed in DMAc

by sonication for 15 min. Then this dispersion was injected into the reaction mixture in the 2nd step of polymerization before completion of the reaction and continued the reaction for another 1 h. The reaction was stopped before the gelation.

xii) Instrumentation and testing

The infrared spectra of the hyperbranched polyurethanes were recorded by impact 410, Nicolet (Madison, USA) Fourier transform infrared (FTIR) spectrophotometer using KBr pellets. Nuclear magnetic resonance (^{1}H-NMR) spectrum of the polymers was recorded by a 400 MHz NMR spectrometer (JEOL, Japan) using d_6-DMSO as the solvent and TMS as an internal standard. The Raman spectra of MWCNT were recorded by Invia Renishaw Raman spectrometer, England. The X-ray diffraction study was carried out at room temperature (ca. 25 °C) by a Rigaku X-ray diffractometer (Miniflex, UK) over a range of 2θ=10-70°. The thermal analysis was done by a Simadzu, Japan thermal analyzer, TG50, with a nitrogen flow rate of 30 mL/min at a heating rate of 10 °C/min. The differential scanning calorimetry (DSC) study was done by DSC 60, Simadzu, Japan at a 3 °C/min heating rate under the nitrogen flow rate of 30 mL/min from −30 to 150 °C. The mechanical properties such as tensile strength and elongation at break were measured with the help of an Universal Testing Machine (UTM), Jinan, China with a 500 N load cell and crosshead speed of 0.05 m/min using sample of dimension: 0.1 m × 0.01 m × 0.00035 m. Scratch resistance of the dry films was measured by using a scratch hardness tester, model number 705 (Sheen instrument Ltd., UK) with stylus accessory and a travel speed of 0.03-0.04 m/s. The impact resistance was measured by an impact tester (S.C. Dey & Co., India, 1.0 m is the maximum height) using the standard ASTM D 1037 falling weight method. A weight of 0.85 kg was allowed to fall on the mild steel plate coated film from minimum to maximum height up to which the film was not damaged. The maximum height was taken as the impact resistance. Raman spectra were taken with SPEX 1403 double monochromator coupled to a SPEX 1442. The samples were excited with an air cooled argon ion laser of wavelength 488 nm. Elemental analysis was done by CHN Analyzer, Model PR 2400 Series II Perkin Elmer.

Shape memory test

Thermo-mechanical cyclic tests were performed to investigate the shape memory effect of the HBPU. These tests consisted of loading the specimen to a strain (ε_m) at a constant crosshead speed of 5 mm min^{-1} at a temperature T_{high} (stage 1), and then cooling down to the temperature T_{low} while holding the same strain ε_m (stage 2). After 5 min at the temperature T_{low}, the specimen was unloaded at same strain. After 5 min at the temperature

T_{low}, the specimen was unloaded (stage 3) and reached a strain ε_c. The unloaded specimen was immediately heated from T_{low} to T_{high} in 5 min (stage 4), which left a permanent strain ε_p high. This four-stage thermo-mechanical cycle was repeated for a total of 4 cycles. The fixed conditions of the cyclic test were: ε_m = 100%; T_{high}= 60°C, and T_{low} = - 20°C, and ε_c (the strain after unloading) and ε_p (the permanent strain) were both recorded for each specimen.

The bending shape memory tests were achieved by folding the sample in ring form at 60 °C followed by quenching into an ice-water bath and finally irradiate it under MW. While irradiating, the shape recovery by the samples was recorded by using a digital camera. The shape recovery and shape fixity were calculated using the following equations.

Shape recovery (%) = $\{(90-\theta)/90\} \times 100$ ---------- (3)

Where θ in degree denotes the angle between the tangential line at the midpoint of the sample and the line connecting the midpoint and the end of the curved samples.

Shape fixity (%) = $(\Delta u/\Delta m) \times 100$ ---------- (2)

Where are the maximum strain (100%) and residual strain after unloading the stress at 0 °C.

Shape memory behavior of pristine HBPU and its nanocomposite also determined by stretching test. At first, film was cut into rectangular strips with the dimension of 0.04 m × 0.005 m × 0.0006 m and heated at 60 °C (T_m + 20 °C) for 5 min. Then it was stretched to twice of their original length (L_0) using a stretching rate of 0.02 m/min and stretched length is denoted as L_1. Immediately, the stretched samples were freezed at 0 to 5 °C (T_m – 40 °C) for 5 min to fix the temporary shape and the length was measured as L_2 after removal of the load. Subsequently, the samples were reheated at the same temperature (60 °C) for the same period of time for the shape recovery and the length obtained is denoted as L_3. The same procedure was followed for the repeated cycles of test. The shape recovery and shape fixity are two shape memory parameters calculated from the following equations:

Shape recovery (%) = $[(L_1-L_3)/L_0] \times 100$ ---------- (3)

Shape fixity (%) = $[(L_2-L_0)/L_0] \times 100$ ---------- (4)

10. Detailed analysis of results indicating contributions made towards increasing the state of knowledge in the subject:

The analyses and discussion of the results are illustrated below-

i) Synthesis of *Mesua ferrea* L. seed oil/castor oil/sunflower oil based hyperbranched polyurethane matrices*

* Parts of this works has been published in –

Polym. Eng. Sci. **2012**, 52, 2454–3461; *Prog. Org. Coat.* **2013**,76, 157–164 **&** Ind. Crop. Prod. **2013**, 44, 396– 404.

The hyperbranched polyurethanes with different oil contents were synthesized by using two step one pot $A_2 + B_3/B_4$ approach. In all the cases the NCO/OH ratio was maintained as one to get high molecular weight. The urethane linkages were formed by the reaction between isocyanate groups of the TDI with the hydroxyl groups of the monoglyceride of oil and PCL.This prepolymer along with unreacted TDI act as A_2 type monomers. In the second step the multifunctional moiety (triethanolamine/ pentaerythritol/ castor oil) was added slowly in a dilute solution at room temperature to avoid gelation. Gelation occurs if the multifunctional moiety added to the mixture at high temperature or at high concentration of reactants. In the second stage, the chain extension of the polyurethane occurs by the reaction of –NCO groups of the prepolymer and unreacted TDI with the hydroxyl groups of multifunctional moiety through with the generation of possible branched structure. After the given time of reaction, the presence of –NCO group was determined by butylamine titration method and FTIR spectroscopic study, which indicate the completion of the reaction, in each case. The whole sequence of reactions is shown in the Scheme 1. Castor oil, sunflower and *Mesua ferrea* L. seed oil based hyperbranched polyurethane are encoded as CHBPU, NHBPU and SHBPU, and without vegetable oil based encoded as HBPU.

Characterization

Fourier Transform Infrared spectroscopy (FTIR)

The FTIR is a powerful spectroscopic technique to observe the conformation, accessibility, extent of hydrogen bonding and interaction between hard-soft segments in case of hyperbranched polyurethane. In this present study the extent of hydrogen bonding is investigated by the changes occurring in the mid-infrared region both in band intensity and frequency shift. As most of the inherent properties like viscosity, glass transition temperature, solubility etc. are strongly influenced by degree of hydrogen bonding present in the polymer, so any factor (like hard segment content), which increases H-bonding is very important to study. The FTIR spectra of all the hyperbranched polyurethanes have

been shown in the Fig. 1. The main peaks of the hyperbranched polyurethanes with their corresponding functional groups are tabulated in the Table 1.

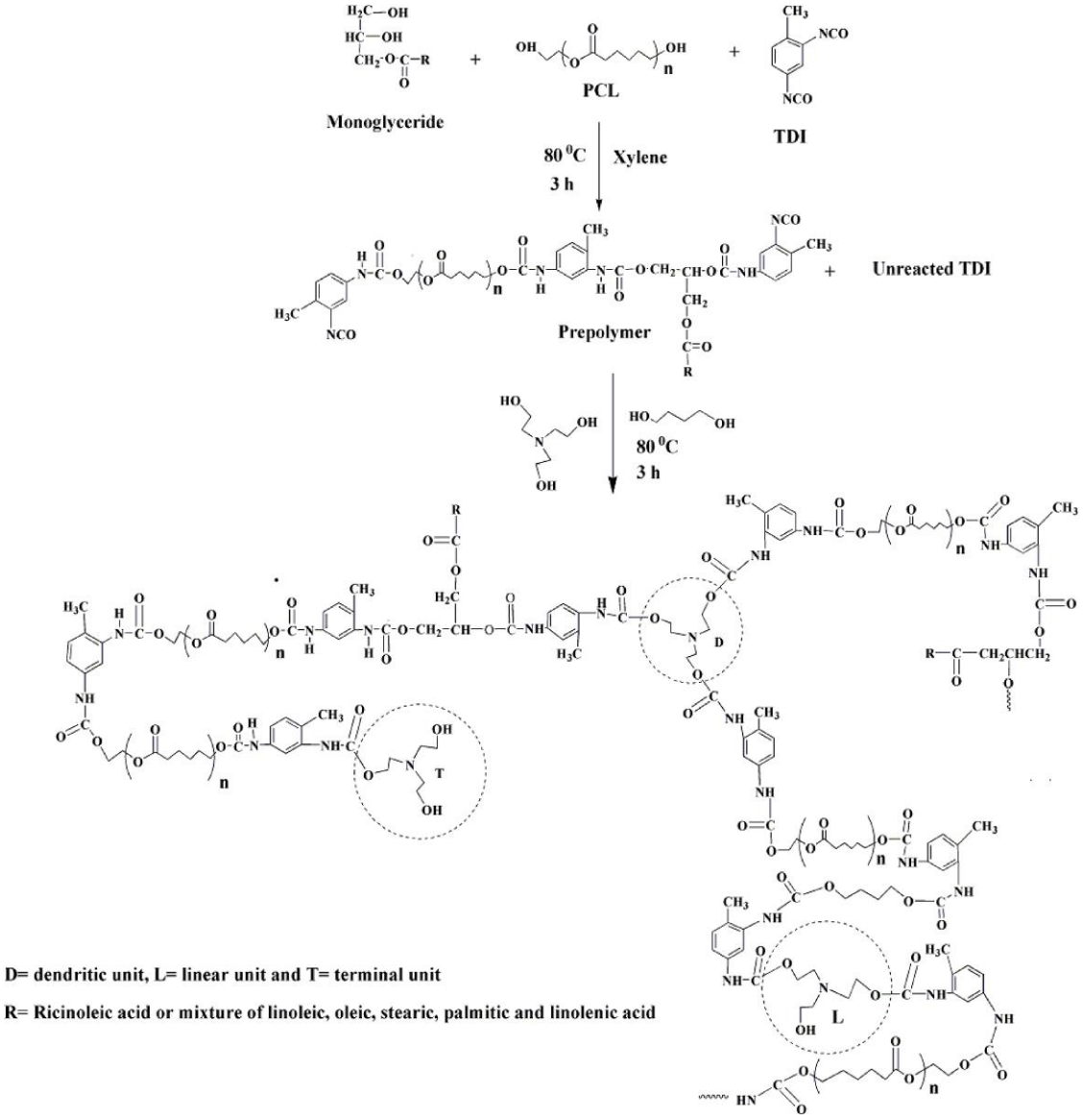

Scheme 1.Synthesis of vegetable oil based hyperbranched polyurethane

The absence of any sharp and intense band at 2250-2270 cm^{-1} proves that there were no free –NCO group present in the polymers which indicate the completion of the reaction. From the shift values of −C=O and –N−H bands to lower wave number regions as compared to the hydrogen free data can be easily detected from IR spectra. The shift value and intensity of the band indicate the magnitude of the H-bonding. The –NH stretching vibration in all the spectra of the polymers appears at about 3409-3438 cm^{-1}, which arises from the H-bonded –NH groups. There are the possibilities to form H-bonding between –NH groups of PU with the urethane carbonyl, the PCL carbonyl.

Table 1 FTIR spectral data of the different bio-based hyperbranched polyurethanes

Band position (cm^{-1})	Functional groups
3409-3438	NH stretching vibrations
2859-2950	CH_2 symmetric and anti-symmetric stretching vibrations
1669-1710	amide I, C=O stretching vibrations
1557-1580	amide II, C-N stretching and N-H bending character
1469-1474	CH_2 scissoring, CH_3 deformation and CH_2 bending
1369	C-H deformation
1045-1050	O-C=O stretching of urethane/ester group
872	C-O stretching and CH_2 rocking

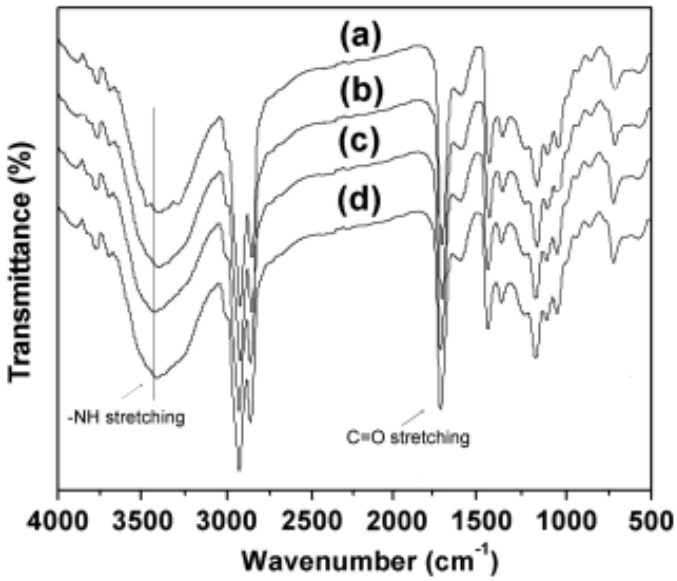

Fig. 1. FTIR spectra for (a) CHBPU, (b) NHBPU, (c) SHBPU, and (d) HBPU

^{1}H NMR spectroscopy

^{1}H-NMR spectra of the different vegetable oil based HBPU are shown in Fig. 2. The peaks at ∂=0.80-0.87 ppm, ∂=1.19-1.27 ppm and ∂=1.47-1.51 ppm are due to the terminal methyl group, all internal $–CH_2–$ groups and the protons for $–CH_2–$ groups attached next to the terminal methyl group of the fatty acid chain of the monoglyceride of the oil, respectively. The protons of allylic $–CH_2–$, $–CH_2–$ adjacent to –O– of urethane

group and – CH_3 of TDI showed peaks at ∂=2.19-2.26 ppm, ∂=2.23-2.27 ppm and ∂=2.40-2.68 ppm, respectively. The $–CH_2–$ protons of triethanolamine moiety attached to the urethane linkages and $–CH_2–$ protons attached to –OH groups were found at ∂=3.1-3.3 ppm and ∂=3.96-4.03 ppm, respectively. The integration ratio of these two peaks indicates the extent of substitution of the –OH of the branch generating moiety, triethanolamine. The observed ratio was found to be 2.50 for the CHBPU10, which indicated that out of three –OH groups, 2.50 groups were substituted i.e. the degree of branching is about 0.83. Similarly, the degree of branching was found to be 0.76. 0.70 and 0.64 for NHBPU10, SHBPU10 and HBPU, respectively. The chemical shifts of protons of aromatic moiety were observed at around ∂=7.7-8.00 ppm. However, there was another peak for castor oil based hyperbranched polyurethane at ∂=3.8 ppm for the –CH− proton attached to the –OH of the ricinoleic moiety. All the above spectral analyses confirmed the formation of hyperbranched polyurethane.

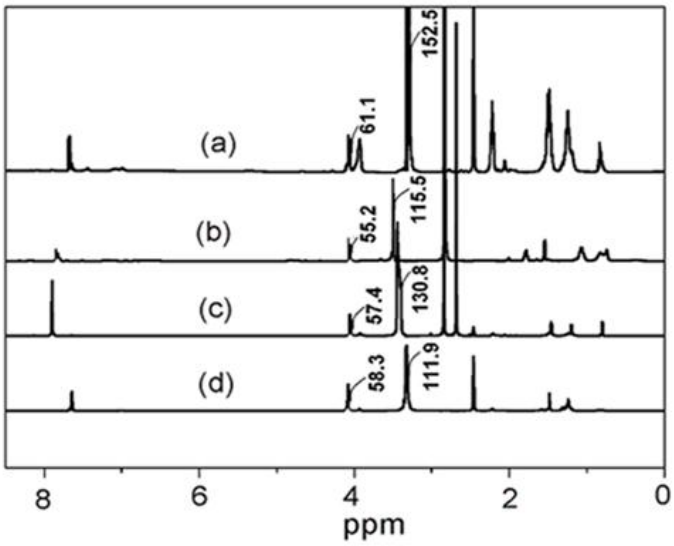

Fig. 2. ^{1}H-NMR spectra for (a) CHBPU, (b) SHBPU, (c) NHBPU, and (d) HBPU.

Physical property

One of the most important characteristic properties of highly branched polymer is its solubility. It is found that the hyperbranched polyurethanes are soluble in the solvents like 1, 4-dioxane, acetone, ethyl acetate, DMF and DMSO. The branched backbone with large number of surface groups along with globular compact, non-entangled structure of the hyperbranched polymers offers rapid dissolution. Other properties like color, inherent

viscosity are given in Table 2. Color of polymer mainly depends on color of oil used for synthesis of the polyurethane.

Table 2 Physical properties of the different bio-based Hyperbranched polyurethanes

Property	NHBPU	CHBPU	SHBPU
Color	Brown	Light Yellow	Light Yellow
Inherent viscosity at 25°C	0.22	0.70	0.80
Degree of branching	0.93	0.65	0.71

XRD Study

XRD study of all the different bio-based hyperbranched polyurethanes were shown in Fig. 3. The presence of crystallinity of the thermoplastic hyperbranched is confirmed by XRD analyses. The two diffraction peaks at $2\theta=21.2^{o}$ (4.19 A^{o}) and 23.4^{o} (3.81 A^{o}) are due to PCL crystals. These two peaks remain same for different bio-based hyperbranched polyurethane, which indicates that extent and nature of crylstallinity of the system remain same for different polyurethanes.

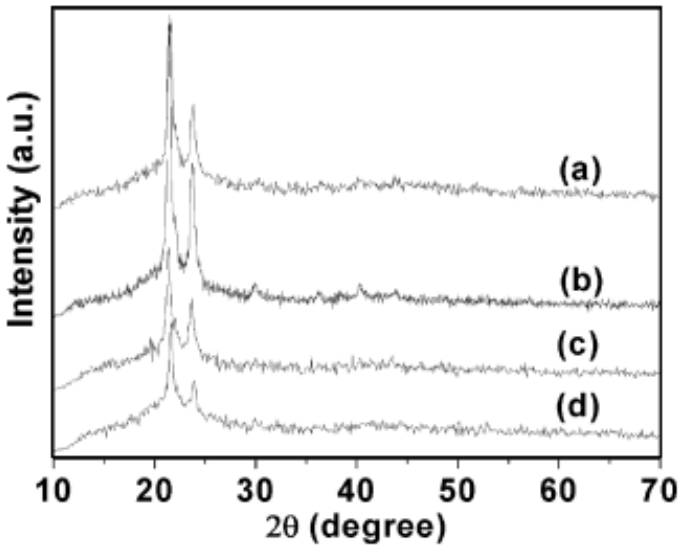

Fig. 3 X-ray diffractograms for (a) CHBPU, (b) NHBPU, (c) SHBPU, and (d) HBPU.

Morphological Properties

The morphological study was done with the help of scanning electron micrographs of the hyperbranched polyurethanes. The Fig. 4 showed the SEM micrographs of polyurethanes of different vegetable oils. The SEM micrographs indicate the uniform phase distribution of the polymers.

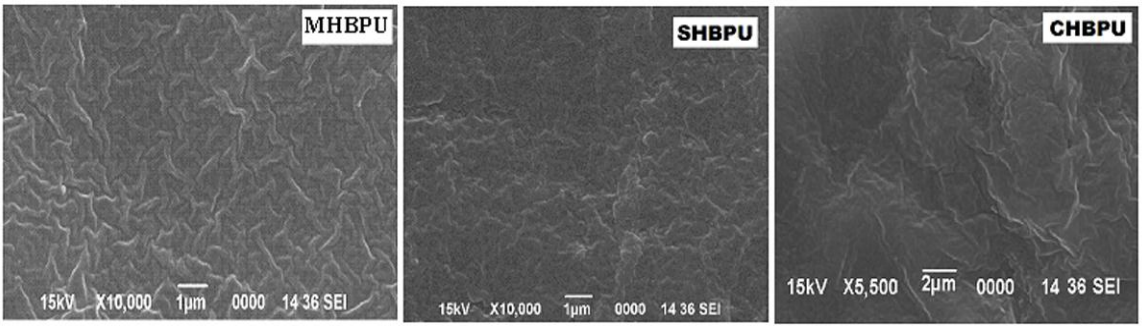

Fig. 4 SEM micrographs of different vegetable oil based HBPU

Chemical resistance

Chemical resistance of all the different bio-based hyperbranched polyurethanes were studied under various chemical environments such as aqueous NaCl (10%), EtOH (10%), HCl (5%), NaOH (3%) solutions and distilled water for 7 days and changes of weights were determine after the tests (Table 3). All the films showed very good chemical resistance in almost all the chemical environments, except NaOH solution. This may due to the presence of the alkali hydrolysable ester groups in the PCL and monoglyceride segments.

Table 3. Chemical resistance as changes of weight (g) of hyperbranched polyurethanes

Code of polyurethane	NHBPU	SHBPU	CHBPU
3% NaOH	−0.071	−0.083	−0.001
10% EtOH	+0.002	+0.001	0.00
5% HCL	−0.003	−0.004	−0.006
10% NaCl	+0.004	+0.034	−0.096
Distilled Water	+0.015	+0.10	−0.002

Thermal Properties

Generally the themostability of polyurethane depend on the number of urethane linkages and presence of aromatic moiety as they can withstand a considerable temperature. Also the linkages such as allophanate and biuret formed at the time of cross linking reactions, presence of secondary interactions increases the themostability of the polyurethane. From the TGA thermograms (Fig. 5) it is observed that all the bio-based polymers undergo two steps degradation. The first degradation may be due to the dissociation of thermo-labile allophanate, biuret linkages and the second one is due to the decomposition of urethane linkages, which are degraded at comparatively high temperature.

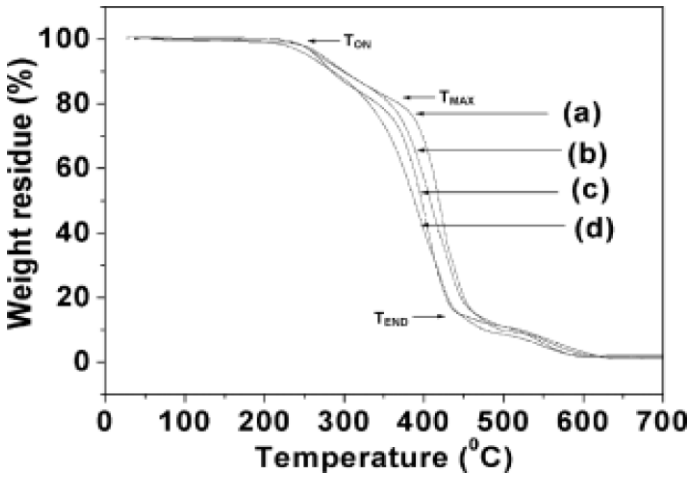

Fig.5 Thermogravimetric analysis thermograms for (a) NHBPU, (b) SHBPU, (c) HBPU, and (d) CHBPU.

Mechanical Properties

The mechanical properties of a polymer depend on its molecular weight, chemical linkages, entanglement, crystallinity etc. In the polyurethane there are two chemically different moieties, viz. hard and soft segment. The hard segment reinforces the internal strength of the polyurethanes and hence the distribution of such segments and interaction between them influence the mechanical properties. The mechanical properties of the hyperbranched polyurethanes are given in Table 4. All the hyperbranched polyurethanes show adequate flexibility as they can be bent to a very low diameter of mandrel. This flexibility is attributed by the flexible PCL ether, ester linkages and the long hydrocarbon chain of the oil. The gloss property is measured for the hyperbranched polyurethanes. These values are comparable to the other resins prepared from this oil. The tensile strength of the nanocomposite is enhanced compared to the pristine polyurethane. This is due to the H-bonding between the functionalized carbon nanotubes and urethane linkages of the polyurethane.

Table 4. Mechanical properties of the different bio-based hyperbranched polyurethanes

Property	NHBPU	CHBPU	SHBPU
Tensile strength (MPa)	12.58	8	16.2
Elongation at break (%)	480	699	726
Scratch hardness (kg)	3.0	4.2	3.5
Bending Test (mm)	< 2	< 2	< 2
Impact Test (cm)	>100	>100	>100
Gloss (60°)	98	74	79.0

However, elongation at break decreases after incorporation of carbon nanotubes in the polymer matrix. This may be due to the increase the rigidity of the polymer. The results indicate the homogenous distribution of Carbon nanotubes in the polymer matrix.

Shape-Memory Study

The shape-memory behaviors of the different hyperbranched polyurethanes are shown in Fig. 6. The samples were stretched above T_m (60°C) of the hyperbranched polyurethanes and were subsequently frozen at a low temperature (0 to 5°C) to fix the deformed shape. The shape fixity temperature of 0–5°C was chosen on the basis of the fact that it could be achieved easily under the experimental conditions that we used and because it was a much lower temperature than the crystalline T_m of the soft segment. The crystalline T_m was considered the switching temperature because the melting transition was sharper than T_g. All of the vegetable-oil-based polyurethanes exhibited good shape fixity; this indicated that the micro-Brownian movements of the molecular chains in the physical network of the soft segment were frozen at the fixing temperature and, thereby, stored the applied load as strain energy. The vegetable-oil-based polyurethanes showed a higher shape fixity than the oil-free polyurethane. This may have been due to the presence of long-chain fatty acid moieties in the structure, which enhanced the secondary interactions during the vitrification. All of the vegetable-oil-based polyurethanes showed good shape recovery, although the castor-oil-based one showed the best shape recovery (Table 5). This could be attributed to the presence of more physical crosslinking due to the higher urethane linkages, which caused the storage of more deformed energy in the system. The sample immediately released the deformed stored energy and returned to its original shape on reheating. The *M. ferrea* L. seed-oil-based hyperbranched polyurethane also exhibited good shape recovery. This may have been due to the presence of various secondary interactions and the highly crystalline region of this hyperbranched polyurethane. No significant change in shape fixity or shape recovery was obtained for any of the hyperbranched polyurethanes for five cycles of testing.

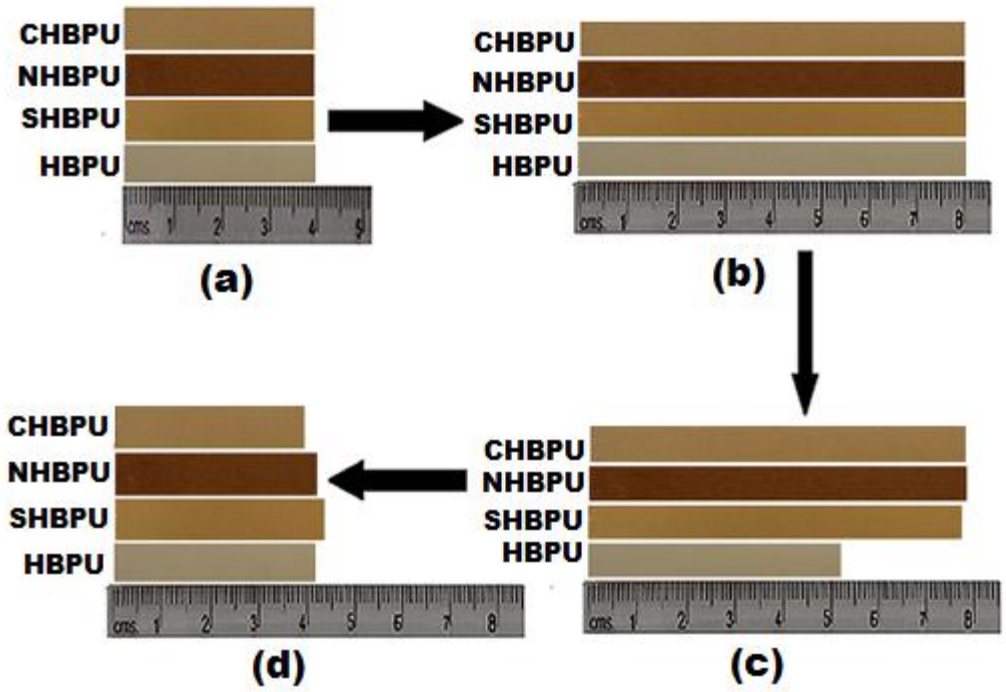

Fig. 6 Shape-memory behaviors of the hyperbranched polyurethanes: (a) original shape, (b) extended shape, (c) fixed shape, and (d) recovered shape

Table 5. Shape-Memory Behavior of the different vegetable oil based HBPU

Sample code	Shape fixity (%)	Shape recovery (%)
CHBPU	98 ± 0.1	98.5 ± 0.2
NHBPU	98 ± 0.2	96 ± 0.1
SHBPU	96.5 ± 0.3	94.8 ± 0.2
HBPU	32.5 ± 0.3	96.5 ± 0.1

Characterization of surface modified MWCNT

FTIR spectroscopy

The FTIR spectra of MWCNT and a-MWCNT are shown in Fig. 7. The FTIR spectra showed that an absorption band at 1726 cm^{-1} (–C=O) was present in a- MWCNT, which was absent in this region for the pristine MWCNT. This confirmed the generation of –COOH group on the surface of MWCNT by the acid treatment.

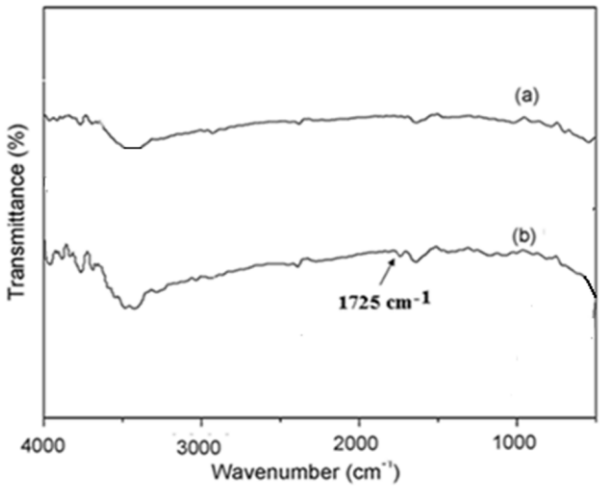

Fig. 7 FTIR spectra for (a) pristine MWCNT and (b) a-MWCNT

Raman spectroscopy

MWCNT and a- MWCNT were further characterized by the Raman spectroscopy. The Raman spectra of pristine MWCNT and a-MWCNT are given in Fig. 8. The Raman spectra of MWCNT showed the D band at 1341 cm^{-1} and G band at 1572 cm^{-1}, whereas the Raman spectra of a-MWCNT showed the D band at 1344 cm^{-1} and G band at 1576 m^{-1}. The D band corresponds to the defect of the MWCNT, while the G band corresponds to the tangential mode of vibrations of the carbon atoms. The intensity ratio between the D band and G band (I_D/I_G) implies the extent of defects of the MWCNT. The value of intensity ratio found to be 0.813 and 0.9 for the pristine MWCNT and a-MWCNT, respectively. This slight enhancement in intensity ratio implies that little defect is generated on the MWCNT after acid treating. The a-MWCNT also showed good dispersion in DMF and remained stable for 2 months, as shown in Fig. 9. This is due to presence of carboxylic groups which polar-polar interaction with solvent molecule. This gives stability of a-MWCNT. However, the pristine MWCNT in DMF settled down after 3h from the time of sonication (Fig. 9).

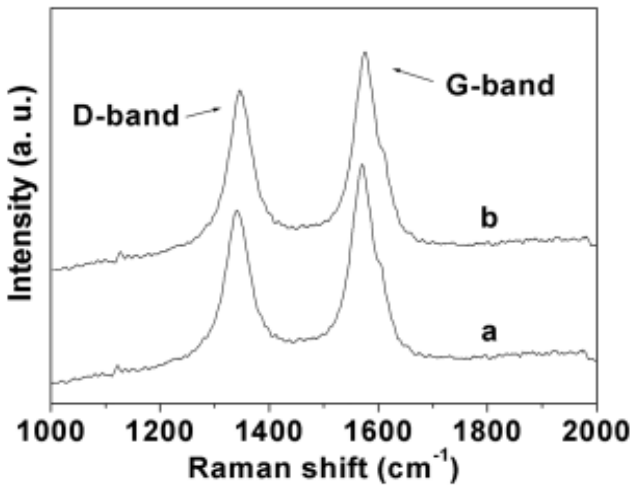

Fig. 8. Raman spectra of (a) a-MWCNT and (b) MWCNT

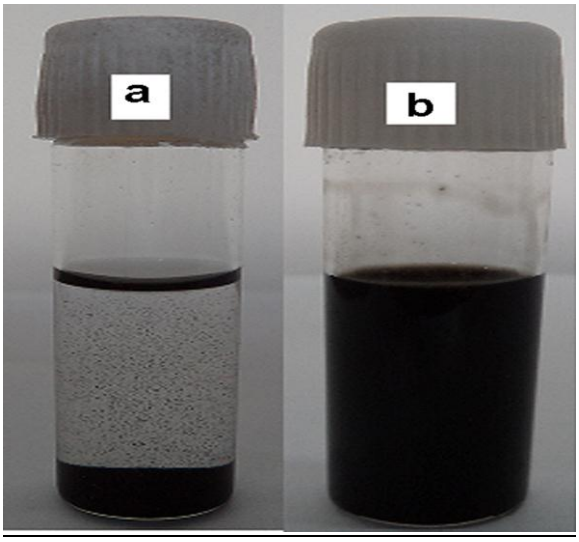

Fig. 9 Dispersion stability of MWCNT in DMF (a) MWCNT and (b) a-MWCNT.

(iii) *Characterization and properties evaluation of triethanol amine functionalized MWCNT (TEA-f-MWCNT)*

FTIR spectroscopy

The spectrum of TEA-f-MWCNT showed the absorption band at 1733 cm^{-1} for –C=O of ester group. In addition the presence of absorption bands at 3146 cm^{-1} (-OH stretching), 2931 cm^{-1} (-CH stretching), 1460 cm^{-1} (-CH bending), 1331 cm^{-1} (C-N stretching) and 1191 cm^{-1} (-C-O of ester group) indicated the functionalized of a-MWCNT by TEA (Fig. 10).

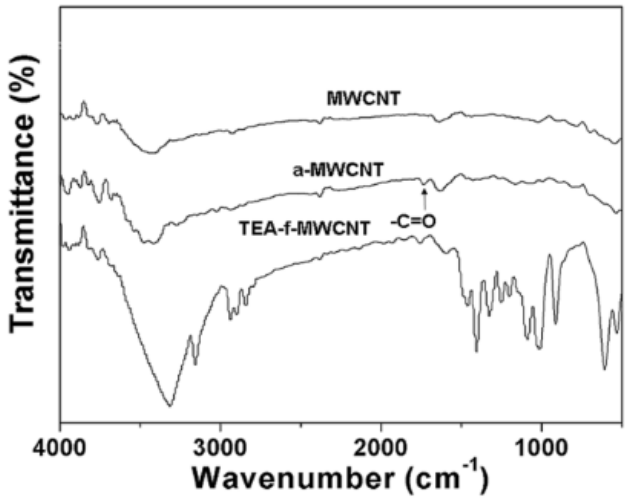

Fig. 10 FTIR spectra of MWCNT, a-MWCNT and TEA-f-MWCNT.

Raman spectroscopy

The functionalization of MWCNT was further characterized by the Raman spectroscopy. Raman spectrum of TEA-f-MWCNT showed the D band at 1340 cm^{-1} and G band at 1570 cm^{-1}. The intensity ratio between the D band and G band (I_D/I_G) implies the degree of covalent functionalization of the MWCNT. The value of intensity ratio found to be 1.11 compared to 0.9 of a-MWCNT. The increase in the value of intensity ratio indicated more defects are generated on the surface of a-MWCNT upon functionalization (Fig. 11).

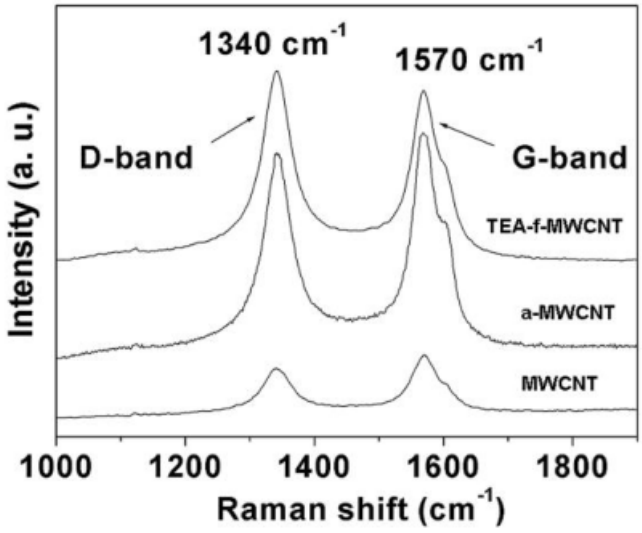

Fig. 11 Raman spectra of MWCNT, a-MWCNT and TEA-f-MWCNT

(iv) ***Characterization and properties evaluation of iron oxide prepared by co-precipitation method***

XRD study

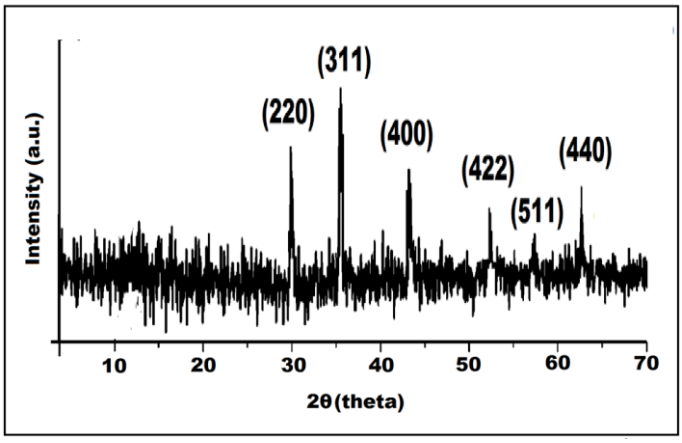

Fig. 12 XRD diffractograms for Fe_3O_4 nanoparticles

The X-ray diffractograms of Fe_3O_4 are shown in Fig.12. The peaks appear at 2θ=30.35°, 35.51°, 56.71° and 62.73° corresponding to (220), (311), (511) and (440) planes of Fe_3O_4, respectively.

Magnetic properties

Fig.13 shows the magnetic hysteresis loops of the Fe_3O_4 at room temperature. From the figure, it is confirmed that the prepared Fe_3O_4 showed the super-paramagnetic behavior.

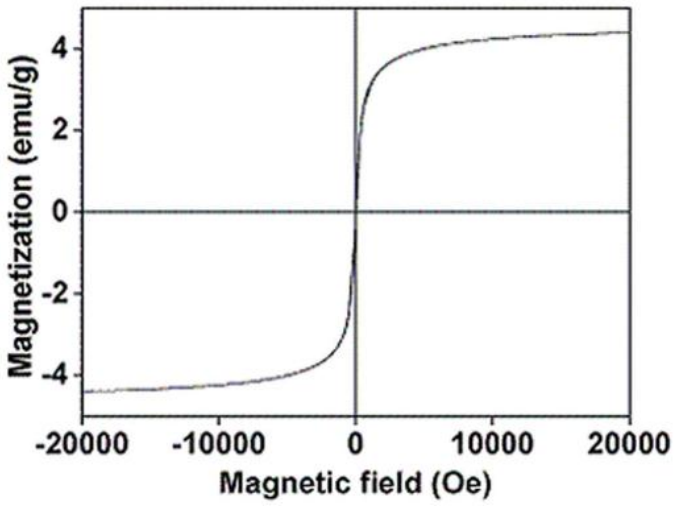

Fig. 13 Magnetic hysteresis loops for (a) Fe_3O_4 nanoparticles

(v) *Characterization and properties evaluation of iron oxide decorated MWCNT (Fe_3O_4-MWCNT)*

FTIR spectroscopy

The FTIR spectra of pristine a-MWCNT, Fe_3O_4 and Fe_3O_4-MWCNT are shown in Fig. 14. The characteristic absorption band observed at 580 cm^{-1} in the spectra of Fe_3O_4 corresponding to Fe-O bending vibration. The band at 3429 cm^{-1} is assigned to the stretching vibration of Fe-OH groups absorbed on the surface of Fe_3O_4 nanoparticles.

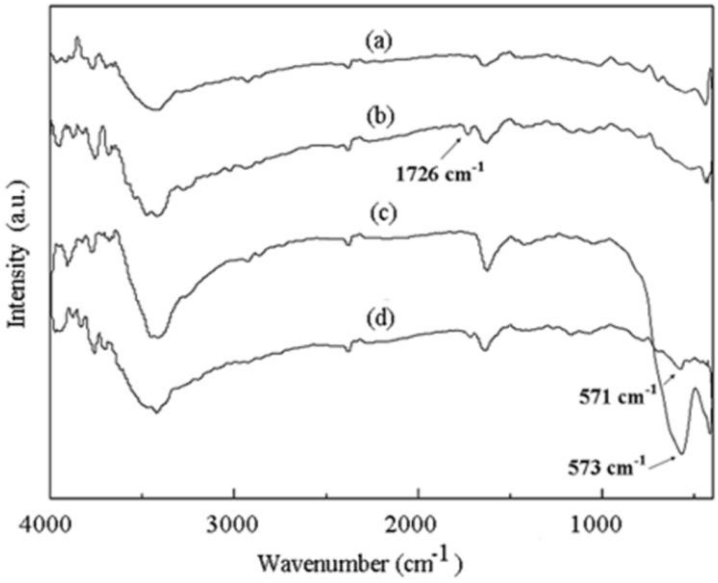

Fig. 14 FTIR spectra for (a) MWCNT (b) a-MWCNT, (c) Fe_3O_4 and (d) Fe_3O_4-MWCNT.

Raman spectroscopy

The Raman spectra of pristine MWCNT, a-MWCNT and Fe_3O_4-MWCNT are shown in Fig. 15. The Raman spectrum of a-MWCNT showed the D and G band at 1341 and 1571 cm^{-1}, respectively, while the Fe_3O_4-MWCNT showed the D and G band at 1352 and 1583 cm^{-1}, respectively.

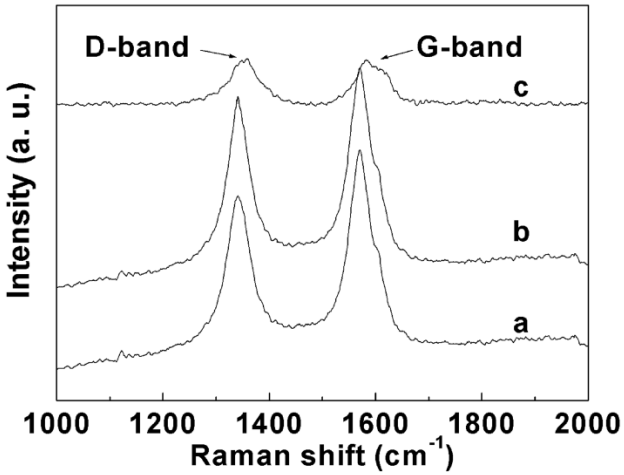

Fig. 15 Raman spectra for (a) pristine MWCNT, (b) a-MWCNT and (c) Fe_3O_4-MWCNT.

(vi) *Characterization and properties evaluation of HBPU/ a-MWCNT nanocomposites*

FTIR spectroscopy

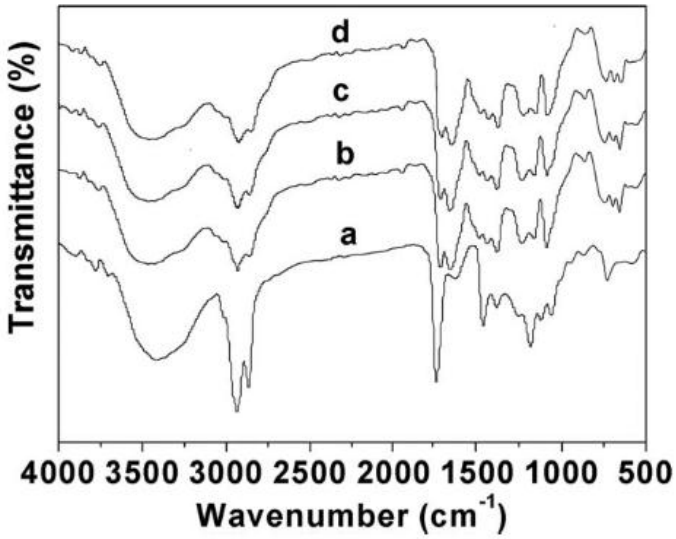

Fig. 16 FTIR spectra of (a) HBPU, (b) NHBPU/ a-MWCNT 0.2, (c) NHBPU/ a-MWCNT 1, and (d) NHBPU/ a-MWCNT 2.

FTIR spectra of the prepared NHBPU/ a-MWCNT nanocomposites are shown in Fig. 16. The characteristic bands of urethane group of pristine polymer appeared at 3406–3430 cm^{-1} (N-H stretching) and 1729 cm^{-1} (—C=O stretching of urethane linkage). The absence of band at 2250–2270 cm^{-1} indicated the absence of free –NCO group in the hyperbranched polymer structure. The intensity of band at 3406–3430 cm^{-1} (N-H

stretching) of nanocomposites decreases and broadens as compared to the pristine polyurethane. Further, the band of –C=O at 1729 cm^{-1} shifted to 1720–1715 cm^{-1} after the nanocomposites formation. All the above results confirmed the presence of strong interaction of a-MWCNT with the polyurethane chains in the prepared nanocomposites.

XRD study

Fig. 17 shows the XRD patterns of the prepared nanocomposites. The peak appears at 2θ=25.4° corresponding to the (002) plane of carbon atoms of MWCNT. There are two strong diffraction peaks at 2θ=21.9° and 2θ=23.8°, which are due to the (100) and (200) planes of PCL crystals of the hyperbranched polyurethane. The peak intensity of the PCL crystal increased after the nanocomposites formation. This is due to the increased crystallinity in the polymer structure. The strong nucleating effect of a-MWCNT may increase the crystallinity in the nanocomposites. However the peak at 25.4° for a-MWCNT is absent in the nanocomposites. This may be due to the low content of a-MWCNT as well as strong interaction between the polymer matrix and the nanomaterial in the nanocomposites.

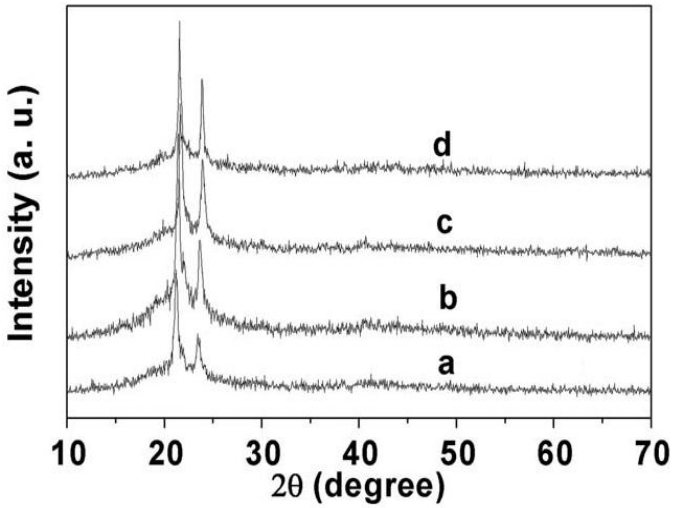

Fig. 17 XRD patterns of (a) NHBPU, (b) NHBPU/ a-MWCNT 0.2, (c) NHBPU/ a-MWCNT 1, and (d) NHBPU/ a-MWCNT 2.

Morphological study

The morphological study of the prepared nanocomposites was carried out with the help of scanning electron micrographs. Fig. 18 shows the SEM micrographs of the hyperbranched polyurethane and the nanocomposites. From these SEM images it is cleared that the surface roughness of the nanocomposites is higher than the pristine polymer system and

also the roughness increases with the increase of a-MWCNT content in the nanocomposites. TEM was used to examine the distribution of a-MWCNT in the nanocomposites. Fig. 19 shows the TEM micrograph of the nanocomposite (NHBPU/a-MWCNT1). This representative TEM image indicated the presence of well dispersed carbon nanotubes with an average diameter 15 nm in the polymer matrix. This well dispersion of the nanotubes in the polymer matrix implies the interaction of nanotubes with molecular chains of the polyurethane. The average diameter of the nanotubes was found to be lesser in the nanocomposites as compared with the pristine carbon nanotubes, which was 18 nm.

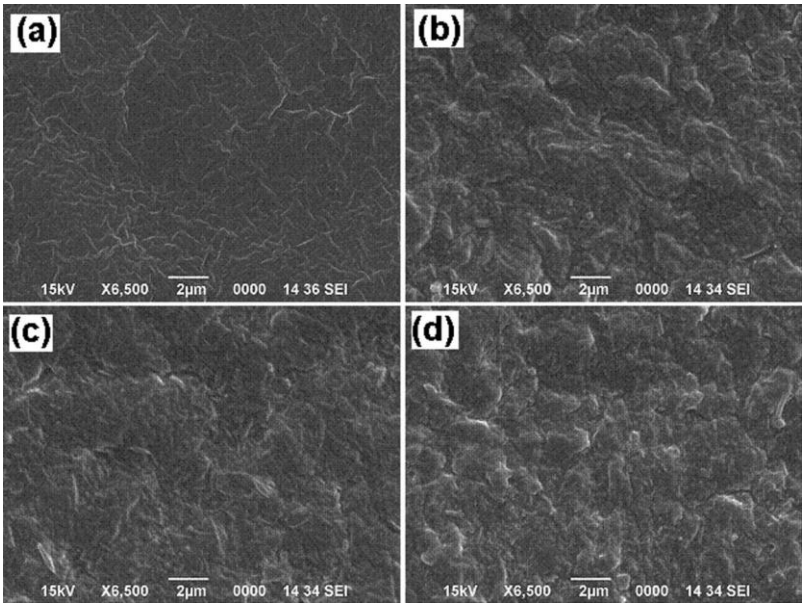

Fig. 18 SEM micrographs of (a) NHBPU, (b) NHBPU/ a-MWCNT 0.2, (c) NHBPU/ a-MWCNT 1, and (d) NHBPU/ a-MWCNT 2.

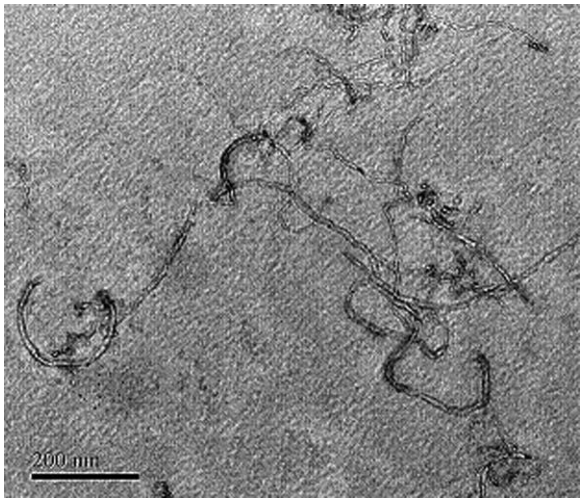

Fig. 19 TEM image of NHBPU/ a-MWCNT 1

Thermal Study

The thermal stability of the prepared nanocomposites was studied by the TGA analysis and the thermo-grams are shown in Fig. 20. The thermal stability of the materials plays a vital role in determining their processing and service temperatures. The thermal stability of the nanocomposites increases with the increase of the amount of a-MWCNT in the nanocomposites. Thermal stability of the nanocomposites depends on the size, shape, nature, loading of nanomaterial, dispersion, and degree of interfacial interaction between the nanomaterial and the polymer matrix. The thermal stability was increased due to the homogeneous distribution of a-MWCNT and enhanced interfacial interaction such as physical cross-linking between the a-MWCNT and the polymer matrix. Therefore, the polymer chains are immobilized on the surface of the nanotubes that causes the restriction of the thermal motion of the macromolecular chains in the nanocomposites. The a-MWCNT act as physical barrier, so the volatile products formed during the thermal decomposition process have to overcome longer zigzag path to escape the matrix. Furthermore, MWCNT are the most thermo-stable and thermal conducting materials, as a result, the increased thermal conductivity of the nanocomposites can assist the dissipation of the thermal energy and thereby thermal stability increased.

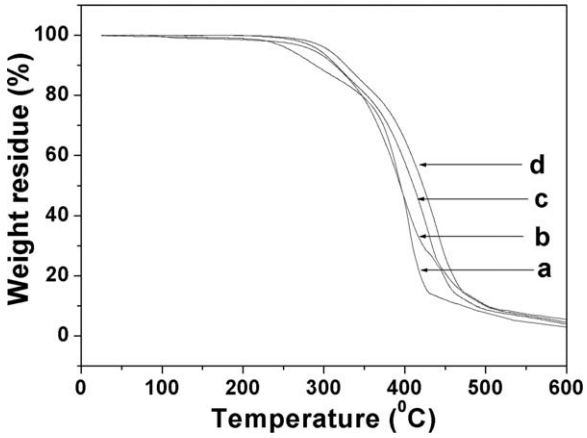

Fig. 20 TGA thermograms of (a) NHBPU, (b) NHBPU/ a-MWCNT 0.2, (c) NHBPU/ a-MWCNT 1, and (d) NHBPU/ a-MWCNT 2.

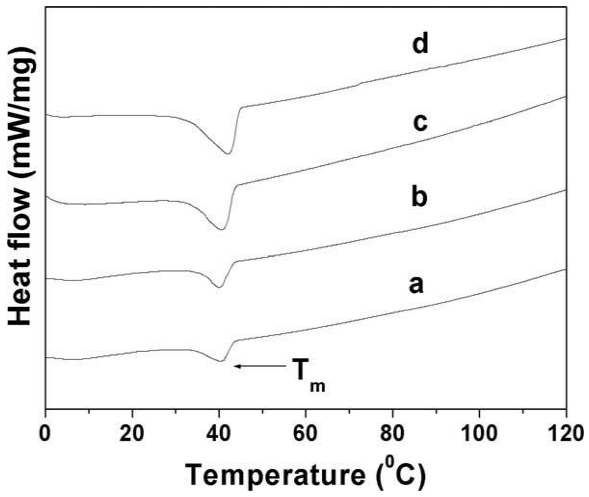

Fig. 21 DSC curves of (a) NHBPU, (b) NHBPU/ a-MWCNT 0.2, (c) NHBPU/ a-MWCNT 1, and (d) NHBPU/ a-MWCNT 2.

Fig. 21 shows the DSC curves of the hyperbranched polyurethane and its nanocomposites. The melting temperature (T_m) was increased (40.1–43.4 °C) with the increase of the content of a-MWCNT in the nanocomposites. This is attributed to the formation of rigid structure as a result of the various interactions between the a-MWCNT and the polymer matrix as stated earlier.

Mechanical Properties

It is expected that carbon nanotubes could act as excellent reinforcing nanomaterials in the polymer nanocomposites owing to its high aspect ratio and high modulus. The tensile strength found to increase with the increase of the amount of a-MWCNT in the nanocomposites (Table 6). This is due to the well distribution of a-MWCNT and the prominent interfacial adhesion between the a-MWCNT and the polymer matrix. The interactions such as hydrogen bonding between the hydrophilic segment of a-MWCNT and the urethane linkages of polyurethane lead to the enhanced stress transfer from the polymer matrix to the carbon nanotubes. However, the elongation at break of the nanocomposites decreases with the increase of the amount of the a-MWCNT (Table 6). This is due to the increased molecular restriction of the polymer chains in the nanocomposites with the increase of a-MWCNT. The scratch resistance of the nanocomposites increases with the increase of the content of a-MWCNT in the nanocomposites (Table 6). This is attributed to the increased overall toughness of the nanocomposites. The prepared nanocomposites exhibited sufficient flexibility as the films could be bent onto a rod of 0.001 m diameter without any crack in the bent films as indicated in the bending test (Table 6). This

indicates retention of flexibility in all the nanocomposites. This is due to the high flexibility of the soft segment and the presence of long chain fatty acid moiety in the structure of the polyurethane. All the films exhibited the good impact resistance. Impact resistance of the material is the ability to absorb the applied external energy as well as the transfer of energy to its adjacent molecular chains.

Table 6. Mechanical properties of hyperbranched polyurethane and its nanocomposites.

Property	NHBPU	NHBPU/ a-MWCNT 0.2	NHBPU/ a-MWCNT 1	NHBPU/ a-MWCNT 2
Tensile strength (MPa)	5.5 ± 0.4	9 ± 0.2	15.2 ± 0.2	21.5 ± 0.2
Elongation at break (%)	690 ± 3.1	480 ± 1.4	445 ± 1.4	415 ± 1.1
Scratch resistance (kg)	3.0 ± 0.1	4 ± 0.1	5.2 ± 0.1	6.1 ± 0.1
Bending (m)	<0.001	<0.001	<0.001	<0.001
Impact resistance (m)	0.95 ± 0.05	0.95 ± 0.05	0.95 ± 0.05	0.95 ± 0.05

(vii) ***Characterization and properties evaluation of NHBPU/ TEA-f-MWCNT nanocomposites***

FTIR study

FTIR spectra of hyperbranched polyurethane and NHBPU/TEA-f-MWCNT nanocomposites are shown in Fig. 22. The characteristic bands of urethane group of pristine polymer appeared at 3406-3430 cm^{-1} (N-H stretching) and 1730 cm^{-1} (-NHCOO- stretching). The disappearance of band 2250-2270 cm^{-1} indicates that there was no free –NCO group present in the hyperbranched polymer structure. The intensity of band at 3406-3430 cm^{-1} (N-H stretching) of pristine polyurethane decreases and broadens after the nanocomposite formation. All the above bands confirmed the interactions of TEA-f-MWCNT with the polyurethane in the prepared nanocomposites.

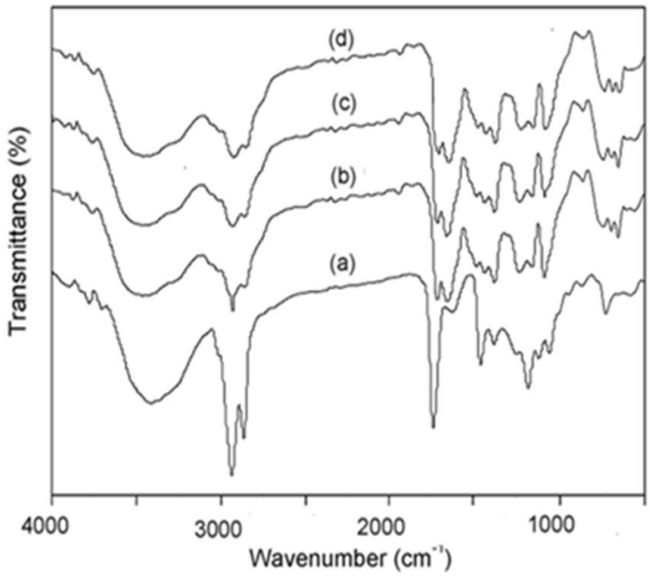

Fig. 22 FTIR spectra for (a) NHBPU, (b) NHBPU/TEA-f-MWCNT0.2, (c) NHBPU/TEA-f-MWCNT1 and (d) NHBPU/ TEA-f-MWCNT2

XRD study

Fig. 23 shows the XRD patterns of hyperbranched polyurethane and all the prepared nanocomposites. The peak appears at 2θ=25.4° corresponding to the (002) plane of carbon atoms of MWCNT. There are two strong diffraction peaks at 2θ=21.9° and 2θ=23.8° due to the (100) and (200) planes of PCL crystals of the hyperbranched polyurethane. The peak intensity increased after the nanocomposite formation. The results showed that the TEA-f-MWCNT serves as nucleating site to increase the crystallinity of hyperbranched polyurethane.

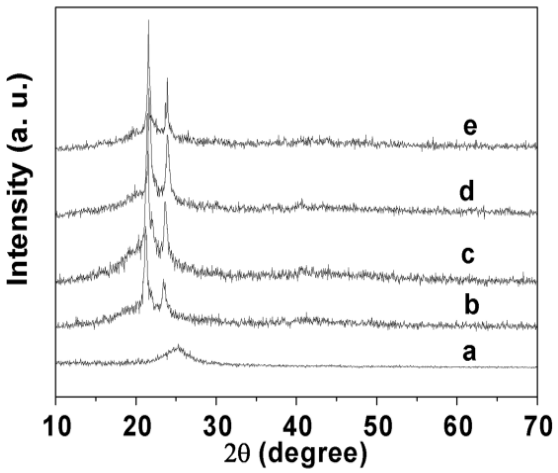

Fig. 23 XRD diffractograms for (a) NHBPU, (b) NHBPU/TEA-f-MWCNT0.2, (c) NHBPU/TEA-f-MWCNT1 and (d) NHBPU/ TEA-f-MWCNT2

Morphology study

Fig. 24 shows the SEM micrographs of the prepared NHBPU/TEA-f-MWCNT nanocomposites. The SEM micrographs indicate the uniform phase distribution of MWCNT in the nanocomposites. This morphology may be due to the good interfacial interaction between the nanoparticles and the polymer matrix. TEM was further used to examine the distribution of MWCNT in the polymer matrix (Fig. 25). The micrograph depicts that MWCNT are well dispersed in the polymer matrix with average diameter 15 nm.

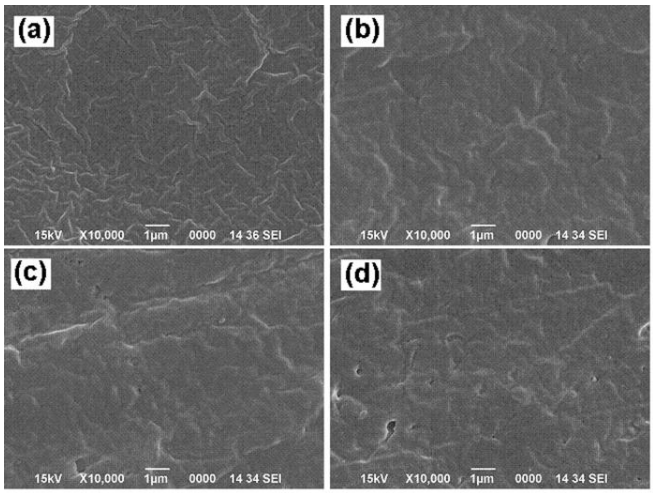

Fig. 24 SEM micrographs for (a) NHBPU, (b) NHBPU/TEA-f-MWCNT0.2, (c) NHBPU/TEA-f-MWCNT1 and (d) NHBPU/ TEA-f-MWCNT2

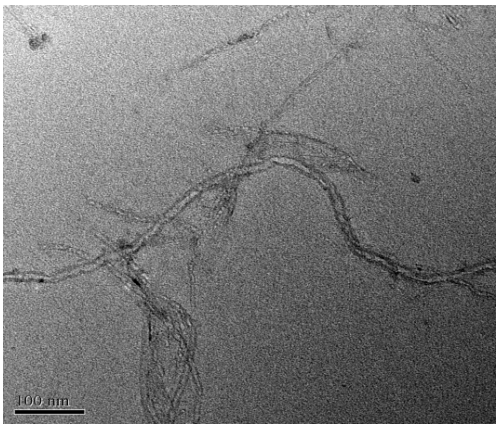

Fig. 25 Representative TEM images for NHBPU/TEA-f-MWCNT1

Thermal study

Thermal stability of the NHBPU/TEA-f-MWCNT nanocomposites increased (241 °C to 284 °C) with the increase of the amount of TEA-f-MWCNT (Fig. 26). This is due to the increased of various physical interactions such as H-bonding and polar-polar interactions along with the chemical bond formation in the nanocomposites. Therefore, the volatile

products formed during the thermal decomposition process have to overcome longer zigzag path to escape the matrix because the well dispersed nanotubes act as gas barrier as well as absorption of free radicals that were generated during the degradation of polymer. Moreover, the molecular mobility of the chains decreases and confers the compactness in the structure of the nanocomposite. As a result, the bond breaking inside the bulk polymeric matrix needs more thermal energy.

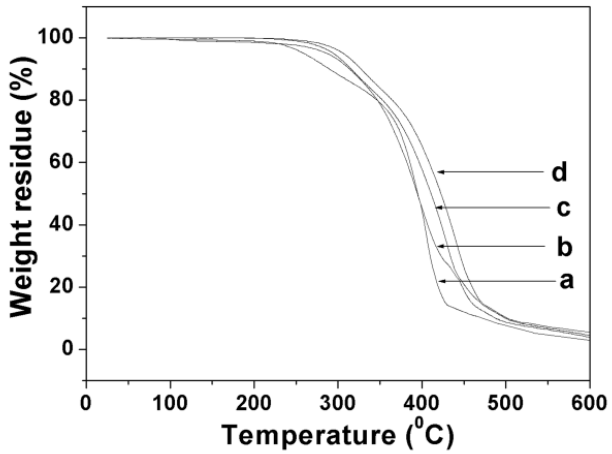

Fig. 26 TGA thermograms for (a) NHBPU, (b) NHBPU/TEA-f-MWCNT0.2, (c) NHBPU/TEA-f-MWCNT1 and (d) NHBPU/ TEA-f-MWCNT2

Mechanical properties

The mechanical properties of the NHBPU/TEA-f-MWCNT nanocomposites are given in Table 7. From the result it is observed that tensile strength increased with the increase of the amount of TEA-f-MWCNT. This is attributed to the increased chemical cross-linking and physical interactions between the TEA-f-MWCNT and the polymer matrix. The interactions such as physical cross-linking of the free –COOH and –OH groups of the nanotubes with the urethane linkages and free –OH of the polyurethane are taken placed. As a consequence they make the material stiffer and lead to the enhanced load transfer from the polymer matrix to the carbon nanotubes. However, the elongation at break of the nanocomposites decreases with the increase of the amount of the TEA-f-MWCNT. This may be due to the increased molecular restriction of the polymer chains physically or chemically on the surface of the MWCNT, resulting in the decrease of flexibility. The scratch resistance of the nanocomposites increased with the increase of the content of TEA-f-MWCNT in the nanocomposite. This may be due to the enhancement of overall toughness of the nanocomposites due the various interactions as stated earlier. The

prepared nanocomposites exhibited sufficient flexibility as the films could be bent onto a rod of 0.001m diameter without any crack in the bent films as indicated in the bending test. This indicates retention of flexibility in all the nanocomposites.

Table 7 Mechanical properties of hyperbranched polyurethane and NHBPU/TEA-f-MWCNT nanocomposites

Property	NHBPU	NHBPU TEA-f-MWCNT0.2	NHBPU TEA-f-MWCNT1	NHBPU TEA-f-MWCNT2
Tensile strength (MPa)	6.5 ± 0.4	13 ± 0.3	20.5 ± 0.3	28.5 ± 0.2
Elongation at break (%)	685 ± 3	480 ± 2	444 ± 2	405 ± 3
Scratch resistance (kg)	3.0 ± 0.1	4.2 ± 0.1	5.5 ± 0.1	7 ± 0.1
Bending (m)	<0.001	<0.001	<0.001	<0.001
Impact resistance* (m)	0.95 ± 0.05	0.95 ± 0.05	0.95 ± 0.05	0.95 ± 0.05

* 1.0 m is the limit of the instrument

Shape memory study

The shape memory behaviors of hyperbranched polyurethane and NHBPU/TEA-f-MWCNT nanocomposites under different stimuli are shown in Fig. 27. The strip like samples of NHBPU/TEA-f-MWCNT nanocomposites was folded to ring structure above the melting temperature (60 ^{0}C) of the hyperbranched polyurethane, subsequently, freezed at low temperature (0 to 5 ^{0}C) to fix the deformed shape. All the prepared nanocomposites exhibited good shape fixity and shape recovery (Table 8). Shape recovery was studied under microwave stimuli. All the nanocomposites showed the excellent shape recovery. However the nanocomposites showed higher recovery time as compared to the pristine polyurethane. This may be due to the increased compactness as well as toughness of the nanocomposites that required more heat to release the stored energy.

Table 8 Shape memory behaviors of hyperbranched polyurethane and its nanocomposites by microwave stimuli

Sample code	Shape recovery (%)	Shape recovery time (s)
NHBPU	100	50 ± 2
NHBPU/TEA-f-MWCNT 0.2	100	55 ± 2
NHBPU/TEA-f-MWCNT 1	100	65 ± 2
NHBPU/TEA-f-MWCNT 2	100	75 ± 2

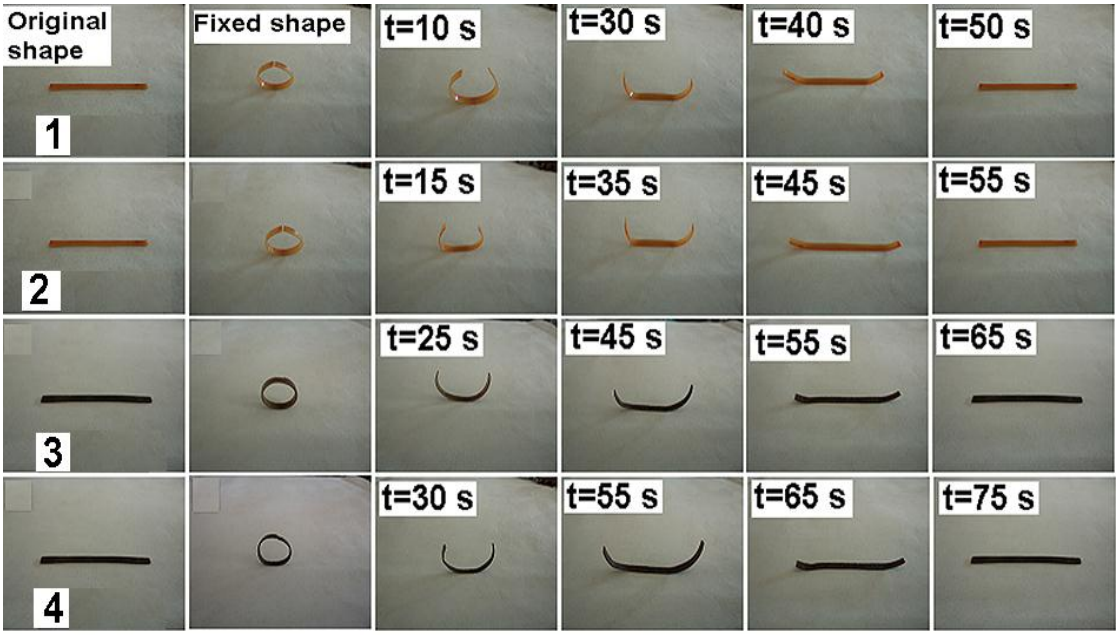

Fig. 27 Shape memory behavior of NHBPU and NHBPU/TEA-f-MWCNT (1) NHBPU, (2) NHBPU/TEA-f-MWCNT 0.2, (3) NHBPU/TEA-f-MWCNT 1 and (4) NHBPU/TEA-f-MWCNT 2

(viii) *Characterization and properties evaluation of NHBPU/ Fe_3O_4 nanocomposites*

FTIR spectroscopy

FTIR spectra of NHBPU and the nanocomposites are shown in Fig.28. The absence of band at 2250–2270 cm^{-1} indicates that there was no free –NCO group present in the NHBPU structure. The band at 3406–3430 cm^{-1} (N–H stretching) of nanocomposites was found to be broadened after the nanocomposite formation as compared to the pristine polyurethane. This confirmed the presence of strong interaction of Fe_3O_4 nanoparticles with the polymer matrix. Further, the characteristic band corresponding to Fe–O of Fe_3O_4 nanoparticles was also broadened after the formation of nanocomposite. This indicates that polymer chains are bound to the surface of the nanoparticles. The above results showed overall strong interactions between the nanoparticles and the polymer matrix.

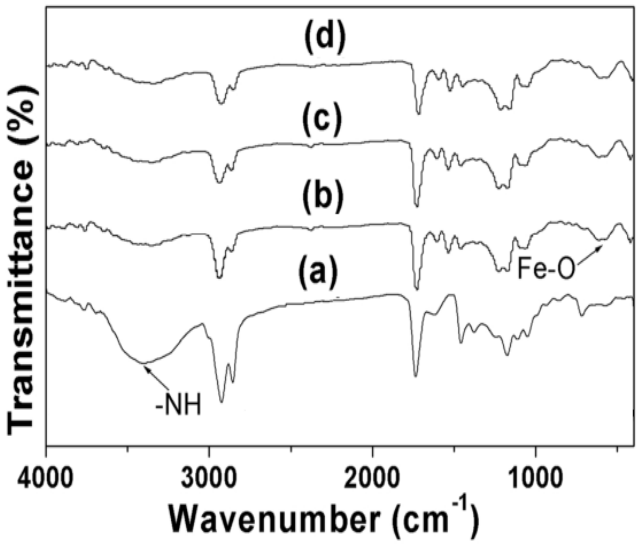

Fig. 28 FTIR spectra for (a) NHBPU, (b) NHBPU/Fe_3O_4-2, (c) NHBPU/Fe_3O_4-5 and (d) NHBPU/Fe_3O_4-10.

XRD study

The X-ray diffractograms of the nanocomposites are shown in Fig.29. There are two strong diffraction peaks at 2θ=21.9° and 2θ=23.8° due to the (100) and (200) planes of PCL crystals of the NHBPU. The intensity of these peaks decreases after the formation of nanocomposite. This may be due to the increased molecular restriction through the different interfacial interactions.

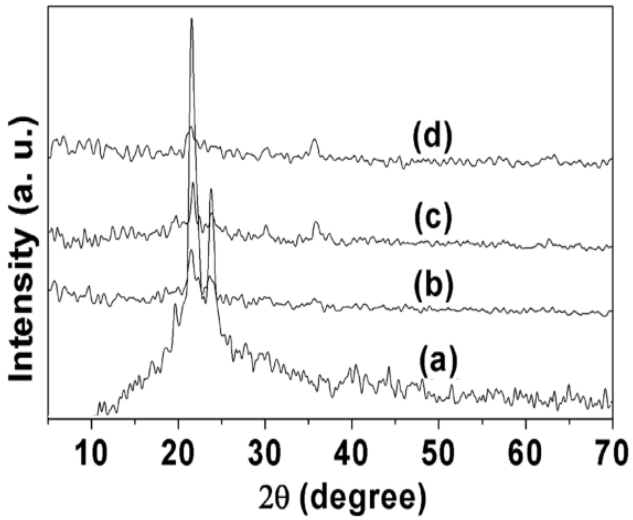

Fig. 29 XRD diffractograms for (a) NHBPU, (b) NHBPU/Fe_3O_4-2, (c) NHBPU/Fe_3O_4-5 and (d) NHBPU/Fe_3O_4-10.

TEM study

The size and distribution of Fe_3O_4 nanoparticles in the polymer matrix were studied by the TEM analysis (Fig.30). The TEM micrograph indicates the homogeneous distribution of

Fe_3O_4 nanoparticles with an average diameter of 13 nm in the polyurethane matrix. This can be attributed to the good interfacial interaction between the nanoparticles and the polymer matrix.

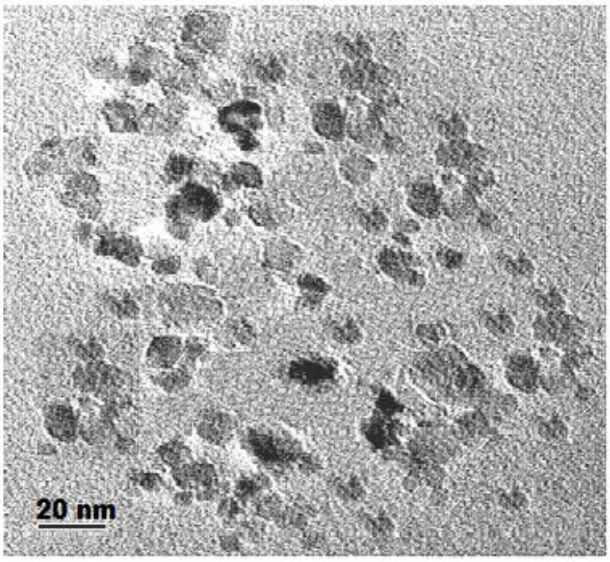

Fig. 30 Representative TEM image of NHBPU/Fe_3O_4-5.

Thermal properties

The thermal stability of the nanocomposites was studied by TGA and the thermograms are shown in Fig. 31. Inorganic compounds are more thermo-stable as compared to the organic polymers. Thermal stability of the nanocomposites depends on the size, shape, nature, loading of nanoparticles, dispersion and degree of interfacial interaction between the nanoparticles and the polymer matrix. Incorporation of Fe_3O_4 nanoparticles into the NHBPU matrix increases its thermal stability (240 to 270 °C). This is due to the uniform distribution, compatibility and strong interfacial interactions of Fe_3O_4 nanoparticles with the polymer matrix. Due to the various interfacial interactions such as physical cross-linking, polar–polar interactions and H-bonding, the polymer chains were immobilized on the surface of the nanoparticles. Thus, the segmental motion of the polymer chains in the nanocomposites was restricted and thereby making the material more rigid. Hence, the bond breaking requires high thermal energy. Furthermore, volatile products formed during the thermal degradation process have to follow a longer path to escape from the matrix.

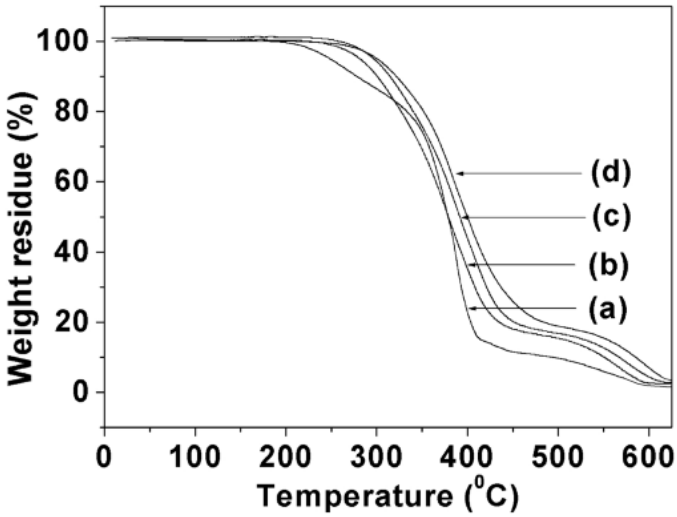

Fig. 31 TGA thermograms for (a) NHBPU, (b) NHBPU/Fe_3O_4-2, (c) NHBPU/Fe_3O_4-5 and (d) NHBPU/Fe_3O_4-10.

Mechanical properties

From Table 9, it is found that nanocomposites possess good mechanical properties viz. tensile strength, impact resistance and scratch resistance along with adequate elongation at break. The mechanical property of the nanocomposite depends on the several factors such as distribution, dimension, aspect ratio of nanomaterials as well as degree of interfacial interactions between the matrix and the nanomaterials. The tensile strength increases with the increase of Fe_3O_4 nanoparticles content in the nanocomposites. This is due to the well distribution and enhanced interfacial interactions of Fe_3O_4 nanoparticles with the polymer matrix. The interfacial interactions increased the load transfer capability of the polymer matrix to the nanoparticles.

However, the elongation at break decreases with the increase of Fe_3O_4 nanoparticles content in the nanocomposites. This is due to the increased molecular restrictions of the polymer chains in the nanocomposites. The scratch resistance of the nanocomposites increases with the increase of the content of Fe_3O_4 nanoparticles. This can be attributed to the overall increase in toughness of the nanocomposites. The bending test results indicated that all the samples have sufficient flexibility as the films could be bent onto a rod of 0.001m diameter without any crack generation. This is mainly due to the high flexibility of the soft segment and the presence of long chain fatty acid moiety in the structure of NHBPU. All the films showed the excellent impact resistance. Impact strength of the material may be explained from the angle of toughness of the films that is the ability to absorb the applied external energy as well as the transfer of energy to its adjacent molecular chains.

Table 9 Mechanical properties of hyperbranched polyurethane and NHBPU/ Fe_3O_4 nanocomposites

Property	NHBPU	NHBPU/Fe_3O_4-2	NHBPU/Fe_3O_4 -5	NHBPU/Fe_3O_4 -10
Tensile strength (MPa)	5.5 ± 0.4	12.2 ± 0.2	13.3 ± 0.2	13.9 ± 0.2
Elongation at break (%)	690 ± 3.1	472 ± 1.4	441 ± 1.4	433 ± 1.1
Scratch resistance (kg)	3 ± 0.1	5.5± 0.1	6 ± 0.1	6 ± 0.15
Impact resistance* (m)	0.95 ± 0.05	0.95 ± 0.05	0.95 ± 0.05	0.95 ± 0.02
Bending (m)	<0.001	<0.001	<0.001	<0.001
Gloss (60^0)	85 ± 2	89 ± 3	89 ± 3	89 ± 3

* 1.0 m is the limit of the instrument

Shape memory study

The shape memory behaviors of hyperbranched polyurethane and NHBPU/Fe_3O_4 nanocomposites under different stimuli are shown in Fig. 32. The shape recovery ratio increases with increase of the concentration of Fe_3O_4 nanoparticles in the nanocomposites (Table 10). This can be attributed to the increased store energy with the loss of elastic entropy as a result of homogeneous distribution of the Fe_3O_4 nanoparticles in the polymer matrix. In the nanocomposites the store internal strain energy is increased due to the increased cross-linking density because the Fe_3O_4 nanoparticles act as a cross-linking agent or net-point. From the above result it is seen that the prepared nanocomposites showed the excellent shape recovery and shape fixity.

Table 10 Shape memory behavior of hyperbranched polyurethane/ Fe_3O_4 nanocomposites

Property	NHBPU	NHBPU/Fe_3O_4- 2	NHBPU/Fe_3O_4 -5	NHBPU/Fe_3O_4 -10
Shape recovery ratio	0.93 ± 0.02	0.96 ± 0.01	0.97 ± 0.01	0.97 ± 0.01
Shape fixity ratio	0.98 ± 0.01	0.99 ± 0.01	0.99 ± 0.01	0.99 ± 0.01

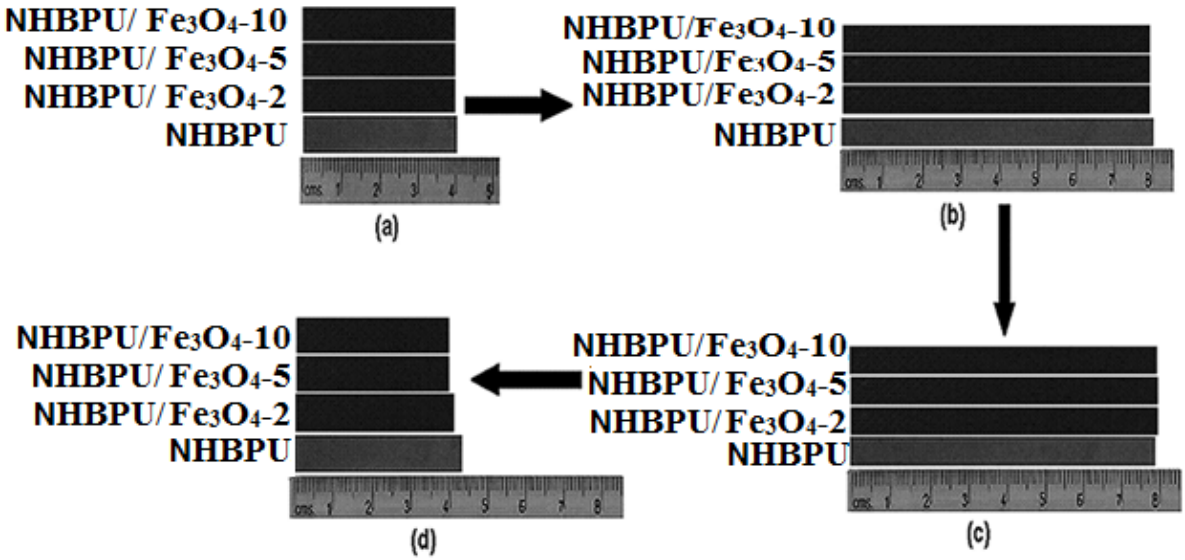

Fig. 32 Shape memory behavior of NHBPU and NHBPU/ Fe_3O_4 nanocomposites (a) original shape and (b) extended shape, (c) fixed shape and (d) recovered shape

(viii) ***Characterization and properties evaluation of NHBPU/Fe_3O_4 nanoparticle decorated MWCNT nanocomposites***

FTIR spectroscopy

The FTIR spectra of NHBPU and the NHBPU/Fe_3O_4-MWCNT nanocomposites are shown in Fig. 33. The characteristic bands of urethane group of pristine polymer appeared at 3406-3430 cm^{-1} (N-H stretching) and 1728 cm^{-1} (-C=O stretching of urethane linkage). The disappearance of band 2250-2270 cm^{-1} indicates that there was no free –NCO group present in the hyperbranched polymer structure. The band at 3406-3430 cm^{-1} (N-H stretching) of nanocomposites was found to broaden after the nanocomposite formation as compared to the pristine polyurethane. Further, the band of –C=O at 1728 cm^{-1} shifted to 1721-1716 cm^{-1} after the nanocomposite formation. All the above results confirmed the presence of strong interactions of Fe_3O_4-MWCNT with the polyurethane chains in the prepared nanocomposites.

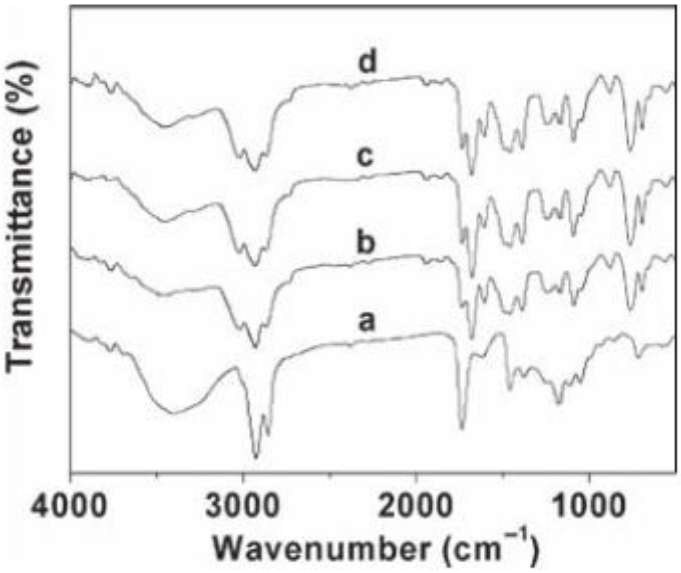

Fig. 33 FTIR spectra for (a) NHBPU, (b) NHBPU/Fe_3O_4-MWCNT 0.2, (c) NHBPU/Fe_3O_4-MWCNT 1 and (d) NHBPU/Fe_3O_4-MWCNT 2.

XRD study

The XRD diffractograms of hyperbranched polyurethane and the nanocomposites are shown in Fig. 34. There are two strong diffraction peaks at 2θ=21.90° and 2θ=23.80° due to the (100) and (200) planes of PCL crystals of the hyperbranched polyurethane. The peaks intensity was found to increase after the formation of nanocomposite. This can be attributed that the Fe_3O_4-MWCNT acts as nucleating site to increase the crystallinity of the hyperbranched polyurethane.

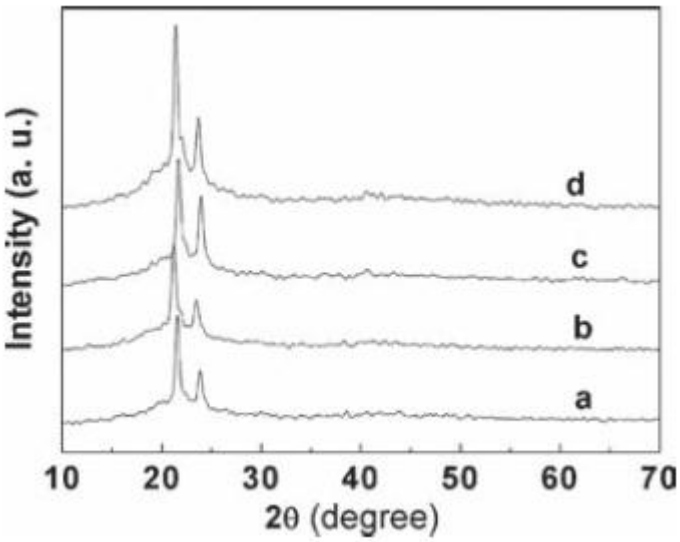

Fig. 34 XRD patterns for (a) NHBPU, (b) NHBPU/Fe_3O_4-MWCNT 0.2, (c) NHBPU/Fe_3O_4-MWCNT 1 and (d) NHBPU/Fe_3O_4-MWCNT 2.

Morphology study

The morphologies of the a-MWCNT, Fe_3O_4-MWCNT and the nanocomposite (NHBPU/ Fe_3O_4-MWCNT1) are shown in Fig. 35. The TEM image of a-MWCNT showed the smooth surface, whereas the Fe_3O_4-MWCNT showed the rough surface. From the TEM micrograph it was observed that Fe_3O_4 nanoparticles are decorated on the surface of the MWCNT. The TEM image of the nanocomposite (NHBPU1) showed the homogeneous distribution of Fe_3O_4-MWCNT in the polymer matrix (Fig. 35 (d)). This is attributed to the good interaction of Fe_3O_4-MWCNT with the polyurethane matrix.

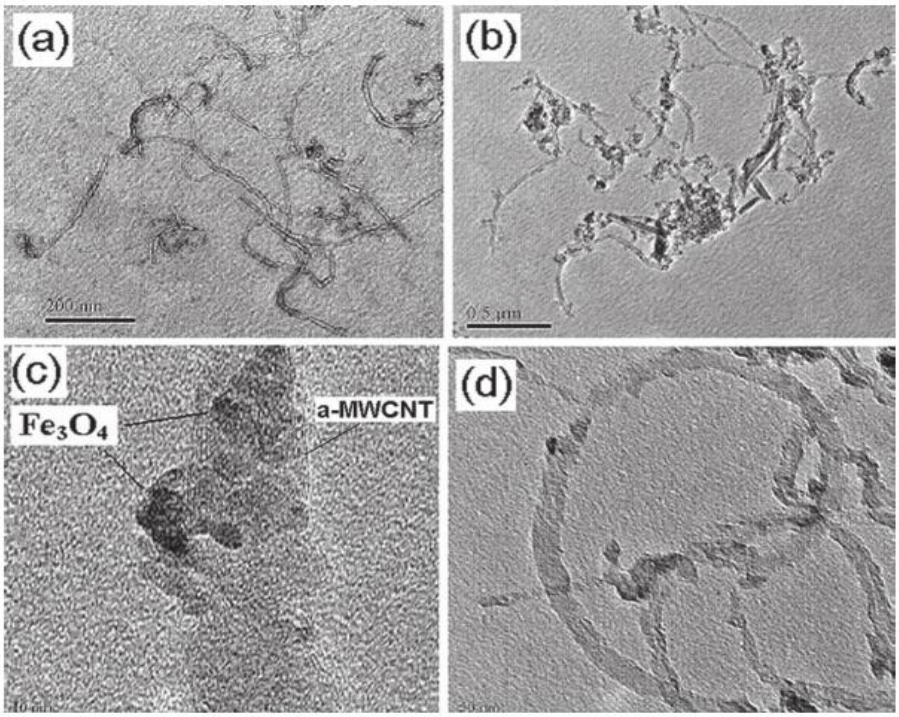

Fig. 35 TEM image for (a) a-MWCNT, (b) and (c) Fe_3O_4-MWCNT, (d) NHBPU/Fe_3O_4-MWCNT 1

Thermal study

The thermal degradation behavior of the prepared nanocomposites was studied by the TGA analysis and the thermograms are shown in Fig. 36. From this figure, it is clear that by increasing the weight percentage of Fe_3O_4-MWCNT increases the thermal stability of the nanocomposites. The onset of the thermal degradation was increased by about 9%, 13% and 18.3% for the nanocomposite with 0.2, 1 and 2 wt% of Fe_3O_4-MWCNT content, respectively. This is due to the decreased in the thermal motion of the polymer chains in the nanocomposites due to the various interactions such as H-bonding, polar-polar interaction between the Fe_3O_4-MWCNT and the polyurethane matrix. Furthermore, the increase in thermal stability of the nanocomposites is due to the homogeneous distribution

of highly thermostable Fe_3O_4-MWCNT that resists the diffusion of volatile products generated during the decomposition process.

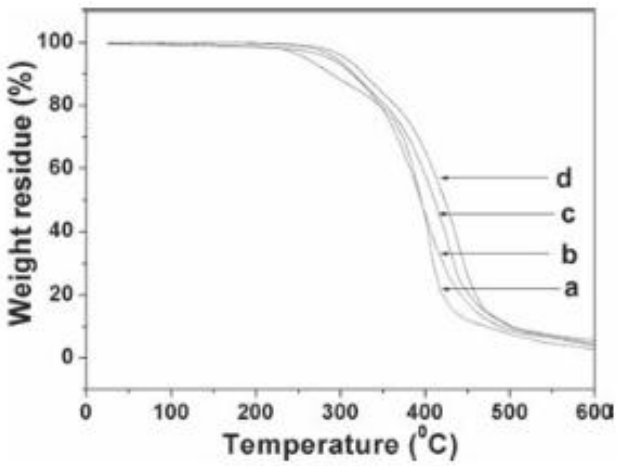

Fig. 36 TGA thermograms for (a) NHBPU, (b) NHBPU/Fe_3O_4-MWCNT 0.2, (c) NHBPU/Fe_3O_4-MWCNT 1 and (d) NHBPU/Fe_3O_4-MWCNT 2.

The DSC curves of hyperbranched polyurethane and the nanocomposites are shown in Fig. 37. From the figure, it is observed that melting temperature (T_m) (39.5 °C to 42.2 °C) of the nanocomposites increased with the increase of the amount of Fe_3O_4-MWCNT. This is due to the increased rigidity of the nanocomposites due to the various interactions between the Fe_3O_4-MWCNT and the polymer matrix.

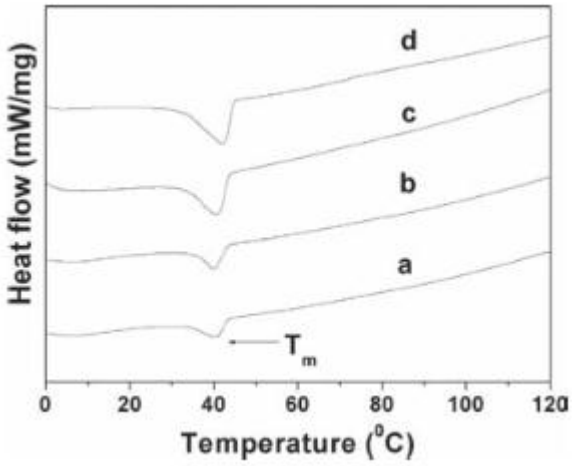

Fig. 37 DSC curves for (a) NHBPU, (b) NHBPU/Fe_3O_4-MWCNT 0.2, (c) NHBPU/Fe_3O_4-MWCNT 1 and (d) NHBPU/Fe_3O_4-MWCNT 2.

Shape memory study

The shape memory behaviors of hyperbranched polyurethane and its nanocomposites under microwave irradiation are shown in Fig. 38. The nanocomposites exhibited good

shape fixity. The micro-Brownian movements of the molecular chains are frozen at low temperature and the applied stress is stored in the fixed shape. All the materials exhibited good shape recovery under exposure of microwave stimulus. When the microwave irradiated on the sample, the dipole moment moves to align with the external electric field components. The oscillations of the dipole field of the molecules, heating effect arises due to the molecular friction and collisions. The polymer chains are activated when the heat is close to the transition temperature (T_{trans}) and release the stored energy to recover the original shape. It was noticed that the shape recovery time decreased with the increase of the concentration of Fe_3O_4-MWCNT in the nanocomposites (Table 11). This can be attributed to the homogeneous distribution of the Fe_3O_4-MWCNT and the increased various interactions with the polymer matrix. Thereby more energy is stored in the system and immediately released the stored energy when the induced heat activated the polymer chains. Moreover the increased shape recovery speed is due to the microwave absorption characteristic of the MWCNT and the Fe_3O_4 nanoparticles.

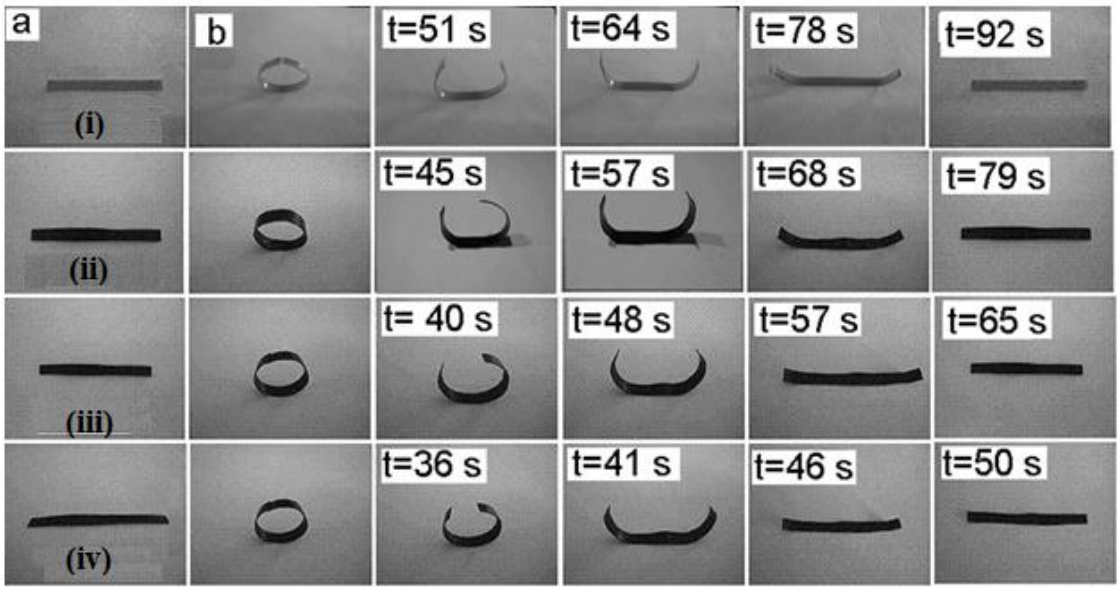

Fig. 38 Shape memory behaviors of (i) NHBPU, (ii) NHBPU/Fe_3O_4-MWCNT 0.2, (iii) NHBPU/Fe_3O_4-MWCNT 1 and (iv) NHBPU/Fe_3O_4-MWCNT 2 under microwave stimulus (a) Original shape and (b) Fixed shape.

Table 11 Shape memory behaviors of hyperbranched polyurethane and its nanocomposites

Sample code	Shape fixity (%)	Shape recovery (%)	Shape recovery time (s)
NHBPU	99± 0.5	98.7±0.5	92±4

Sample code	Shape fixity (%)	Shape recovery (%)	Shape recovery time (s)
NHBPU/Fe_3O_4-MWCNT 0.2	99.5±0.2	99.53±0.2	79±2
NHBPU/Fe_3O_4-MWCNT 1	99.5±0.2	99.53±0.1	65±2
NHBPU/Fe_3O_4-MWCNT 2	99.5±0.2	99.53±0.2	50±2

(ix) ***Characterization of GO and RGO***

FTIR study

FTIR spectra of GO and RGO are shown in Fig. 39. The presence of intense bands at 1720 cm^{-1} (for C=O stretching), 1204 cm^{-1} (for C–O–C stretching), 1049 cm^{-1} (for C–O stretching) and a broad band at around 3400 cm^{-1} for hydroxyl group indicate the presence of oxygen containing moieties such as carbonyl, carboxylic, epoxy and hydroxyl in GO. The removal of such oxygen-containing groups of GO in RGO are clearly indicated by disappearance of the bands of C=O stretching, C–O–C stretching, C–O stretching and relative decrease in the intensity of broad band at 3400 cm^{-1} for the hydroxyl group.

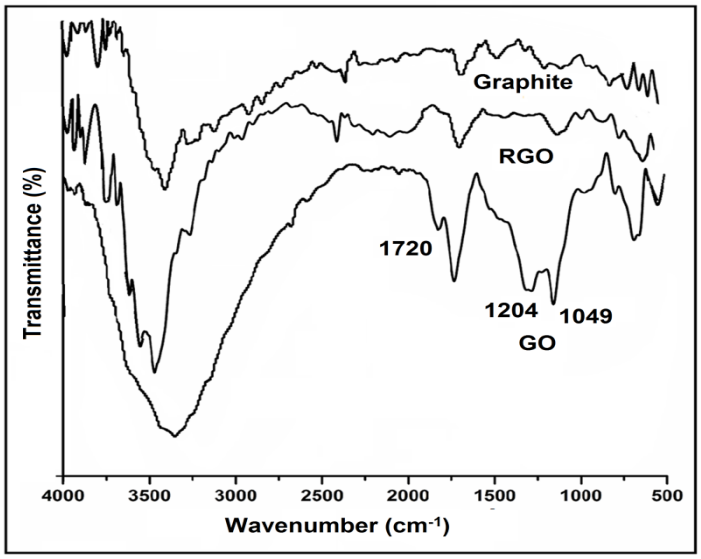

Fig. 39 FTIR spectra of graphite, GO and RGO.

XRD study

XRD patterns of graphite, GO and RGO are shown in Fig. 40. Pristine graphite exhibits a basal reflection [002] peak at $2\theta = 26.6^{o}$ corresponding to d spacing of 0.335 nm. Upon oxidation of pristine graphite, the [002] reflection peak shifts to the lower angle at $2\theta =$

9.75°, (d spacing = 0.906 nm). The increase in d spacing is due to the intercalation of water molecules and the formation of oxygen containing functional groups between the layers of the graphite. In contrast to GO, RGO have a broad peak centred at 2θ = 25° corresponding to d spacing of 0.36 nm which may be due to restacking of graphene layers. The close d-spacing of RGO to pristine graphite and disappearance of peak at 2θ = 9.75° indicates that the oxygen containing group of GO have been efficiently removed. In both GO and RGO, a less intense peak at 43° was observed due to [001] plane of graphene.

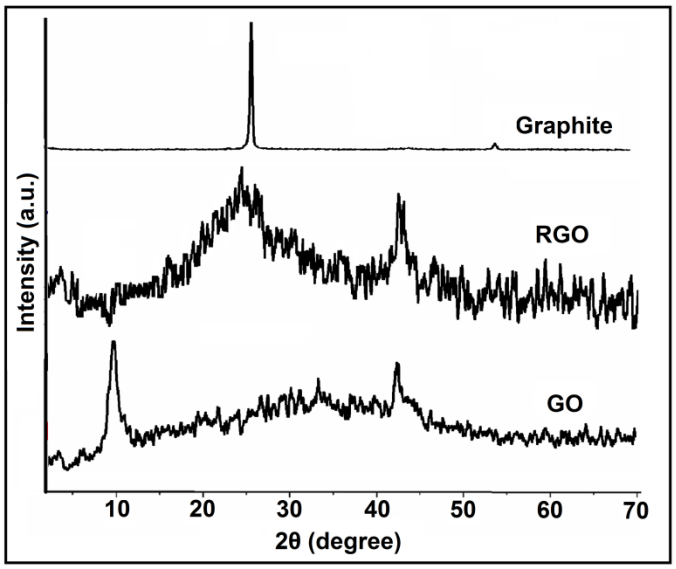

Fig. 40 XRD patterns of graphite, GO and RGO.

Raman study

In graphite and graphene materials Raman scattering is a useful tool to characterize them as this scattering strongly depend on the electronic structure. Raman spectra of GO was significantly changed after reduction (shown in Fig. 41). In the spectra of GO and RGO, two fundamental vibration bands were observed in the range of 1100 to 1700 cm^{-1}. The G vibration mode, owing to the first-order scattering of E_{2g} phonons by sp^2 carbon of GO and RGO were found 1587 and 1584 cm^{-1} respectively while the D vibration band come from a breathing mode of κ-point photons of A_{1g} symmetry of GO and RGO appeared at1322 and 1327 cm^{-1} respectively. After reduction of GO the intensity ratio of the D band to the G band (I_D/I_G) increased significantly. As D band arises due to sp^2 carbon cluster, higher intensity of D band suggested presence of more isolated graphene domain in RGO in compared to GO and removal of oxygen moieties.

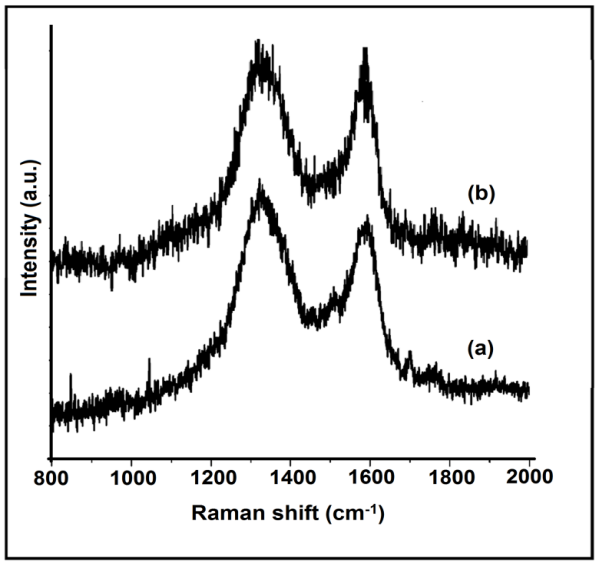

Fig. 41 Raman spectra for (a) GO and (b) RGO

TEM analysis

HRTEM micrographs of RGO are shown in Fig. 42. Fig. 42a shows a silk like appearance of RGO after reduction. Further, from Fig. 42b it is cleared that RGO platelet is almost 5.3 nm thick and consisting of 14 layers. So, interlayer distance is almost 0.37 nm which is in agreement with the XRD result.

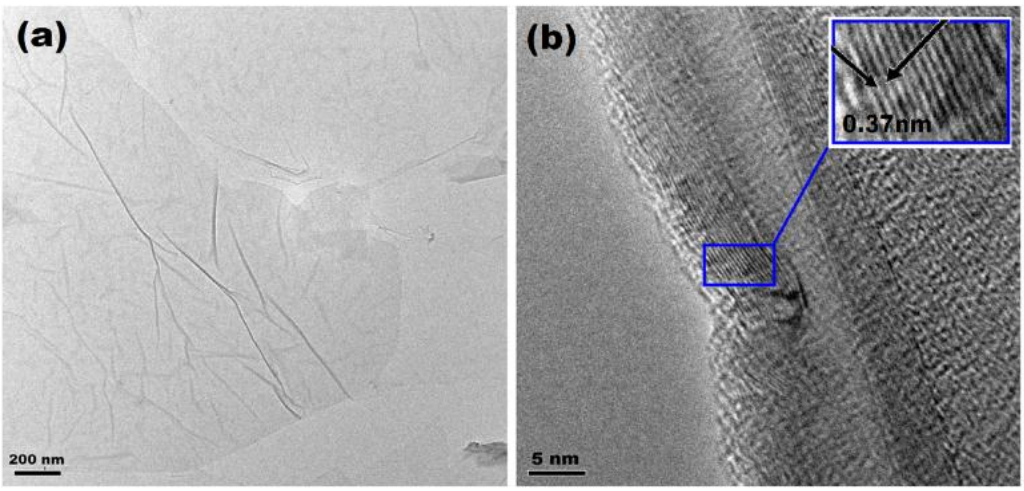

Fig. 42 HRTEM image of RGO at different resolution (a) 200 nm and (b) 5 nm.

Thermal study

Thermal stability of GO and RGO were examined by TGA (Fig. 43). Both GO and RGO showed no significant weight loss near 100 ^{o}C, as the samples were completely dried before testing to eliminate the influence of absorbed moisture on the test results. GO

exhibits two steps degradation; the first step commencing at 175 ^{o}C due to the loss of hydroxyl, epoxy functional groups and remaining water molecules. The second step degradation (450–550 ^{o}C) involves the pyrolysis of the remaining oxygen-containing groups as well as the burning of ring carbon. RGO exhibits only a 7-8 wt% loss upto 250 ^{o}C, which was much lower than that of the GO, indicating a significantly decreased amount of oxygenated functional groups. RGO experiences 20% less weight loss in the 1st step of degradation than GO which is also an indication of degree of reduction.

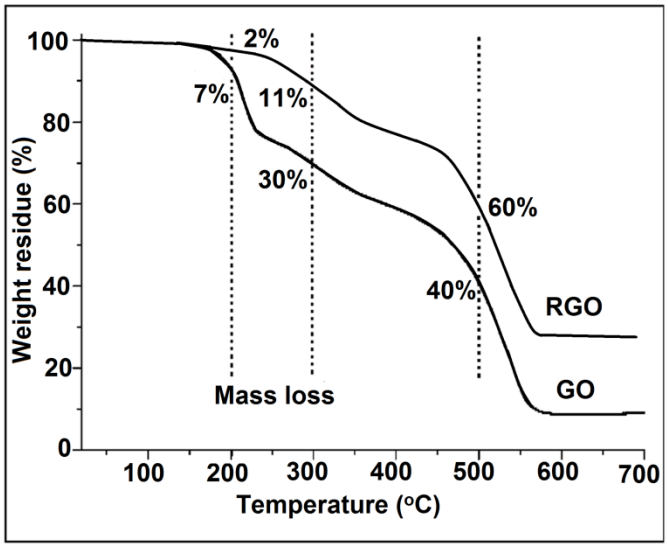

Fig. 43 TGA thermo-gram of graphite GO and RGO.

(x) ***Synthesis, characterization and properties evaluation of CHBPU/GO nanocomposites***

Vegetable oil based CHBPU-GO nanocomposites were prepared by one pot pre-polymerization technique using monoglyceride of castor oil as multifunctional moiety. The important factors for successful preparation of CHBPU are the monitoring of the ratio of functionalities, reaction time, temperature and addition of triol. To obtain high molecular weight CHBPU, the NCO/OH ratio was kept 1 for all the cases. Here, addition of the reactants was carried out at low temperature under high dilute condition to avoid gelation. As GO contains large amount of oxygen containing reactive functionalities, there is a chance to form gel. Therefore, GO was incorporated at room temperature before 1h of the reaction to be completed and followed by completion of reaction at elevated temperature. The stable dispersion of GO in the CHBPU matrix was observed which indicates good dispersion stability of GO is due to unique branched architecture of CHBPU, which can make GO to permeate into the polymer chains and results polar-polar interaction between

urethane chain and variety of functionality of GO. It is pertinent to mention here on reduction of GO such interaction reduced to a considerable extent as number of such polar groups decreased drastically. The CHBPU-GO nanocomposites were optically homogeneous with an incremental brownish black colour which indicated that the CHBPU could be used to disperse GO effectively.

FTIR study

FTIR was employed to investigate the linkages between GO and CHBPU. In Fig. 44, the incidence of intense bands at 1720 cm^{-1} (for C=O stretching), 1204 cm^{-1} (for C–O–C stretching), 1049 cm^{-1} (for C–O stretching) and a broad band at around 3400 cm^{-1} for hydroxyl group indicated the presence of oxygen containing moieties such as carbonyl, carboxylic, epoxy and hydroxyl in GO. The presence of characteristic band at 1060–1090 cm^{-1} (C - N stretching vibrations), 1140–1175 cm^{-1} (C–O stretching vibrations), 1557–1580 cm^{-1} (C-N stretching and N-H bending character), 1601–1635 cm^{-1} (C=C stretching vibration) 1690–1720 cm^{-1} (C=O stretching vibrations from urethane groups), 2859–2950 cm^{-1} (CH_2 symmetric and anti-symmetric stretching vibrations) and 3430 cm^{-1} (O–H free and N -H stretching from urethane group stretching vibrations) clearly reflected the formation of urethane linkage, -NH-C(=O)-O- in CHBPU and its nanocomposites. The increasing amount of GO in the nanocomposites enhances the broadening of –OH band and shifts C=O band to 1690 from 1720 cm^{-1}. These suggest the interaction between CHBPU and GO was enhanced with GO concentration.

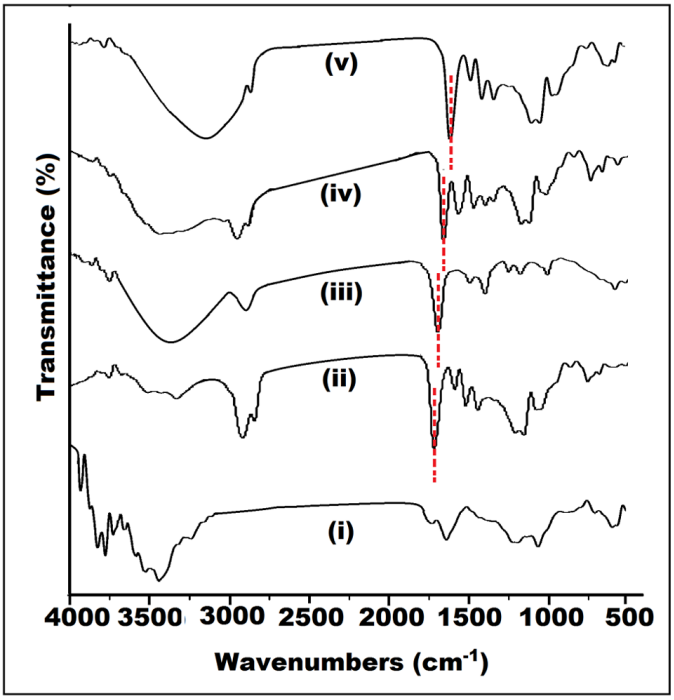

Fig. 44 FTIR spectra of (i) GO, (ii) CHBPU, (iii) CHBPU-GO0.5, (iv) CHBPU-GO1 and (v) CHBPU-GO2.

XRD study

The XRD patterns of GO, CHBPU-GO0.5, CHBPU-GO1and CHBPU-GO2 are shown in Fig. 45. GO showed two peaks at 2θ value 9.84° and 43° for (002) and (001) planes. In contrast to GO, the CHBPU and nanocomposites showed two peaks at 2θ = 21.1° (d spacing = 4.19 A°) and 23.4° (d spacing = 3.81 A°) for the crystals of PCL moiety. It is noteworthy that no such peak of GO was found in the nanocomposites. This reflects that no long range order was present in the GO sheets, or that the distance between the sheets (caused by the exfoliation of the matrix PU) was too large to provide a signal. In addition to that small amount of GO was used for nanocomposite which may be another reason for this. The peak intensity of PCL moiety also increased with the increased of amount of GO due to the strong nucleating effect of the GO and enhancement of interaction between GO and CHBPU. In nanocomposites, PCL peaks were little shifted towards higher angle owing to formation of the dense structure compared to pristine CHBPU.

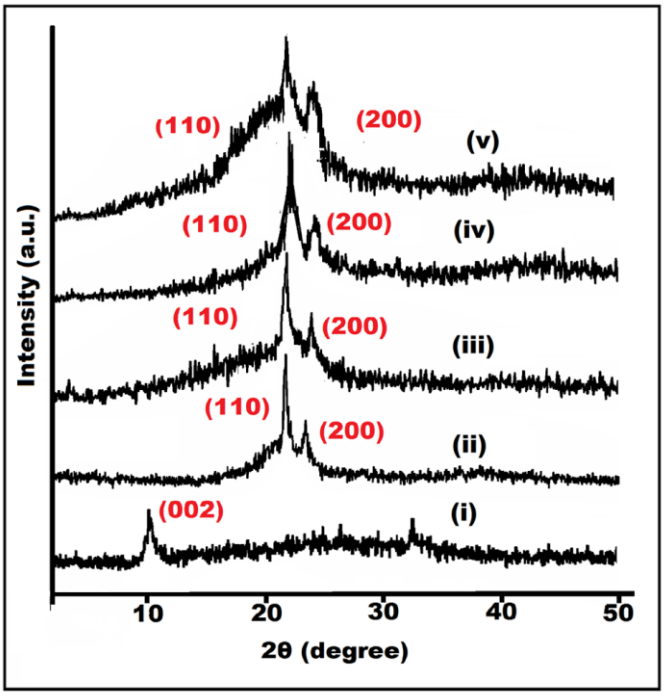

Fig. 45 XRD patterns of (i) GO, (ii) CHBPU, (iii) CHBPU-GO0.5, (iv) CHBPU-GO1 and (v) CHBPU-GO2.

Mechanical properties

Fig. 46 represents the stress–strain curves of the neat CHBPU and its nanocomposites. All the films showed nonlinear elastic behavior within the low stress region and high plastic deformation under high stress. The most outstanding feature is that the nanocomposites exhibited enhance elongation at break over the neat CHBPU. The pristine CHBPU film exhibited fracture strength (σ_B), tensile modulus (E), elongation at break (ε_B) and toughness (T) of 7 MPa, 2.84 MPa, 695% and 2540.5 MJ/m^3, respectively. After the incorporation of 2% of GO these values were enhanced to 16 MPa, 5.55 MPa, 810% and 6807.6 MJ/m^3. The detailed results are listed in Table 12. It shows that the most efficient improvement came from the 2 wt% GO, which reveals the increment of 128%, 95% and 167% in σ_B, E and T, respectively. It indicates that incorporation of GO as an effective nanomaterial, the resistance against mechanical deformation can be reinforced along with enhancement of the elongation for the nanocomposites. Better mechanical properties such as tensile modulus and strength for the CHBPU-GO nanocomposites could be due to good interfacial interaction upon uniform dispersion of the GO in the CHBPU matrix. There is a possibility of direct linkages between various oxygenating groups of GO and CHBPU chains by physico-chemical interactions. This greatly enhance the compatibility of GO with CHBPU matrix. Thus it becomes favourable to transfer stress to GO and has improved the mechanical strength of the nanocomposite. The presence of immobilized or partially mobilized polymer phase as a consequence of such interactions and orientation of GO and the polymer chain along the direction of tensile flow have a great contribution to the observed enhancement of tensile strength. Further with increment of GO amount, the surface area of such nanomaterials increases which enhances the above factors and thereby improved the mechanical properties. Elongation at break increases with the increase of amount of GO in the nanocomposites.

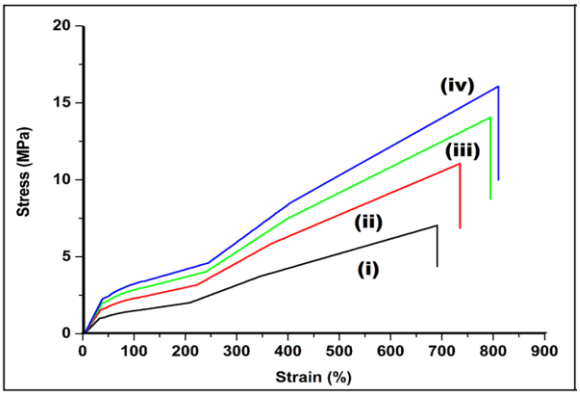

Fig. 46 Tensile curves of (i) CHBPU, (ii) CHBPU-GO0.5, (iii) CHBPU-GO1 and (iv) CHBPU-GO2.

Table 12 Mechanical properties of the CHBPU and nanocomposite films

Sample	CHBPU	CHBPU-GO0.5	CHBPU-GO1	CHBPU-GO2
σ_B (MPa)[a]	7.06 ±1.3	11.23± 2.2	14.05±2.8	16.11±3.1
E (MPa)[b]	2.84±0.2	4.2±0.25	4.85±0.37	6.55±0.32
ε_B (%)	695±43	735±57	795±36	810±46
T (MJm^{-3})[c]	2540±128	4247±164	5845±108	6807±211
Scratch hardness (kg)	5±0.2	5.5±0.1	5.5±0.2	6.5±0.2
Impact strength (cm) [d]	>100	>100	>100	>100

[a] Defined as the stress at the fracture point. [b] Obtained from the slopes of linear areas in stress–strain curves. [c] Calculated by integrating stress–strain curves. [d]The limit of the impact strength was 100 cm (highest).

Shape memory study

The shape memory behaviours of the CHBPU-GO are shown in Fig. 47. The shape memory behavior of material mainly depends on two fundamental factors (i) occurrence of quantitative amount of unlocked orientated polymer chains and (ii) the modulus at room temperature. All polymeric chains experience the same level of deformation when an external force is applied to stretch the sample. The produced deformation is memorized by crystallization or orientation of the soft segment. However, the 'unlocked' chains, the chain segments which do not crystallize generate an instantaneous retractive force upon removal of the tensile load due to entropy of elasticity. Nevertheless, this retractive force alone is insufficient to instantaneous recovery of the shape as the fraction of mobile chains is usually low. The instantaneous retractive force can cause only limited instantaneous recovery strain if the room temperature modulus is high. On the other hand, a more rapid recovery occurs if the value of modulus is low. Switching temperature was selected as 50 ^oC which was about 30 ^oC above T_g and close to the T_m to obtain the best results. The cyclic thermomechanical shape memory behaviour of CHBPU-GO 2 are shown in Fig.48.

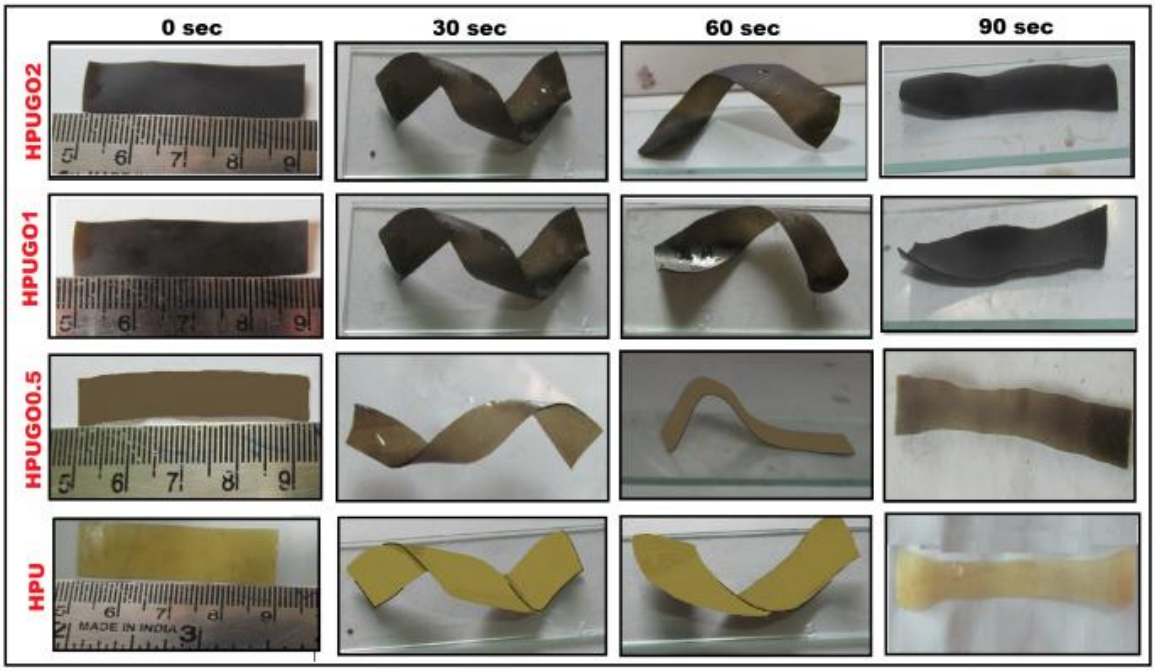

Fig. 47 Shape memory behaviors of castor oil based CHBPU and CHBPU-GO nanocomposites.

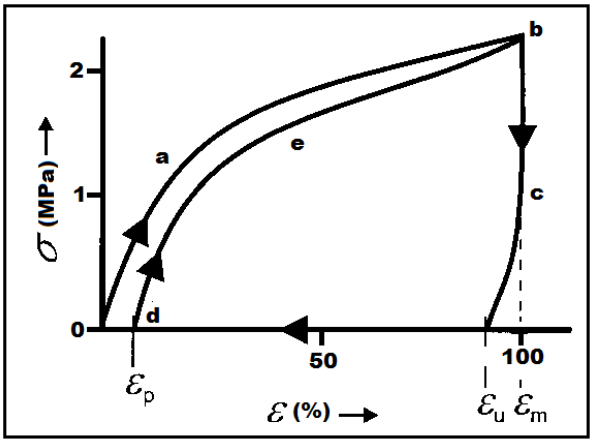

Fig. 48 The cyclic thermomechanical shape memory behaviour of CHBPU-GO 2.

11. Conclusions summarizing the achievements and indication of scope for future work:

From the present investigation following conclusions have been drawn.

(i) *Mesua ferrea* L. seed, sunflower and castor oil based HBPU was successfully synthesized by an $A_2 + B_3/B_4$ approach without gel formation. Among the various hard and soft segment ratios, 30% hard segment containing HBPU showed the optimum performance and hence this ratio was utilized for further studies.

(ii) The conventional analytical and spectroscopic techniques were utilized to characterize the synthesized HBPUs.

(iii) The modification of MWCNT (a-MWCNT) with the acid mixture significantly improved the dispersibility of MWCNT in various solvent.

(iv) HBPU/a-MWCNT nanocomposites were successfully prepared by *in-situ* techniques. The nanocomposites exhibited improvements in performance characteristics.

(v) The a-MWCNT was successfully functionalized with triethanolamine (TEA) to achieve TEA-*f*-MWCNT. The conventional analytical and spectroscopic techniques were utilized to characterize the TEA-*f*-MWCNT.

(vi) NHBPU/TEA-*f*-MWCNT nanocomposites were successfully prepared by *in-situ* techniques. Formation of the nanocomposites caused tremendous improvement in performance characteristics of the conventional polyurethane elastomer. These nanocomposites also exhibited excellent shape memory behavior.

(vii) Iron oxide nanoparticles were successfully prepared by co-precipitation method using ammonia solution as base source. The conventional analytical and spectroscopic techniques were utilized to characterize prepared iron oxide nanoparticles.

(viii) NHBPU/Fe_3O_4 nanocomposites were successfully prepared by *in-situ* techniques. The nanocomposites exhibited excellent shape memory behavior and improvement in performance characteristics of the conventional polyurethane elastomer.

(ix) Fe_3O_4 decorated a-MWCNT and its NHBPU nanocomposites were successfully prepared and characterized by various spectroscopic tools. The nanocomposites exhibited excellent shape memory behavior and mechanical properties.

(x) Graphene oxide (GO) was prepared from graphite by modified Hummer's method and reduction of it was carried out by aqueous phytoextract. GO and reduced GO were well characterized with different analytic and spectroscopic tools.

(xi) CHBPU/GO nanocomposites were successfully prepared by *in-situ* polymerization techniques. The nanocomposite exhibited excellent shape memory behavior and mechanical properties.

Future Directions

Though the present investigation acclaim the successful completion of the pre-set objectives at the same time it opens up few avenues to explore such as-

i) To evaluate or to make some theoretical modeling with the help of computational chemistry of the nano-reinforcing effect.

ii) Study on the nature and extent of H-bonding in the nanocomposites by using different spectroscopic techniques to understand the structure-property relationship, comprehensively

iii) Evaluation of *the* nanocomposites for different biomedical applications through *in-vivo* test.

iv) Development of waterborne polyurethane nanocomposites

v) To evaluate or develop greener and easy root to prepare the nanocomposites etc.

Bibliography

1. Kunzelman, J., et al. Shape memory polymers with built-in threshold temperature sensors, *J. Mater. Chem.* **18** (10), 1082-1086, 2008.

2. Sokolowski, W., et al. Medical applications of shape memory polymers, *Biomed. Mater*. **2** (1), 23-27, 2007.

3. Lu, H., & Gou, J. Fabrication and electro-active responsive behavior of shape–memory nanocomposite incorporated with self-assembled multiwalled carbon nanotube nanopaper, *Polym. Adv. Technol*. **23** (2), 1529-1535, 2012.

4. Xue, L., et al. Synthesis and characterization of three-arm poly(ε-caprolactone)-based poly(ester−urethanes) with shape-memory effect at body temperature, *Macromolecules* **42** (4), 964-972, 2009.

5. Metzger, M., et al. Mechanical properties of mechanical actuator for treating ischemic stroke**,** *Biomed. Microdevices* **4** (2), 89-96, 2002.

6. Liu, C., et al. Review of progress in shape-memory polymers, *J. Mater. Chem.* **17** (16), 1543-1558, 2007.

7. Dietsch, B., & Tong, T. A review: features and benefits of shape memory polymers (SMPs), *J. Adv. Mater.* **39** (2), 3-12, 2007.

8. Gunes, I.S., & Jana, S.C. Shape memory polymers and their nanocomposites: a review of science and technology of new multifunctional materials, *J. Nanosci. Nanotechnol.* **8** (4), 1616-1637, 2008.

9. Mano, J.F. Stimuli-responsive polymeric systems for biomedical applications, *Adv. Eng. Mater.* 10 (6), 515-527, 2008.

10. Ratna, D., & Karger-Kocsis, J. Recent advances in shape memory polymers and composites: a review, *J. Mater. Sci.* 43 (1), 254-269, 2008.

11. Schmaljohann, D. Thermo and pH-responsive polymers in drug delivery, *Adv. Drug Deliver. Rev.* 58 (15), 1655-1670, 2006.

12. Sharp, A.A., et al. Toward a self-deploying shape memory polymer neuronal electrode, *J. Neural. Eng.* **3** (4), 23-30, 2006.

13. Chen, M.C., et al. Rapidly self-expandable polymeric stents with a shape-memory property, *Biomacromolecules* **8** (9), 2774-2780, 2007.

14. Lendlein, A., & Langer, R. Biodegradable, elastic shape-memory polymers for potential biomedical applications, *Science* **296** (5573), 1673-1676, 2002.

15. Small, W., et al. Biomedical applications of thermally activated shape memory polymers, *J. Mater. Chem.* **20** (17), 3356-3366, 2010.

16. Luo, X., & Mather, P.T. Preparation and characterization of shape memory elastomeric composites, *Macromolecules* **42** (19), 7251-7253, 2009.

17. Lu, X.L., et al. Shape memory effects of poly (L-lactide) and its copolymer with poly (ε-caprolactone), *Polym. Bull*. **58** (2), 381-391, 2007.

18. Kang, S.M., et al. Carbon nanotube reinforced shape memory polyurethane foam, *Polym. Bull.* **70** (3), 885-893, 2013.

19. Wu, L., et al. Synthesis, properties, and light-induced shape memory effect of multiblock polyesterurethanes containing biodegradable segments and pendant cinnamamide groups, *Biomacromolecules* **12** (1), 235-241, 2011.

20. Lee, K.M., et al. Light-activated shape memory of glassy, azobenzene liquid crystalline polymer networks, *Soft Matter* **7** (9), 4318-4324, 2011.

21. Chen, S., et al. Novel moisture-sensitive shape memory polyurethanes containing pyridine moieties, *Polymer* **50** (19), 4424-4428, 2009.

22. Schmidt, A.M., et al. Electromagnetic activation of shape memory polymer networks containing magnetic nanoparticles, *Macromol. Rapid. Commun*. **27** (14), 1168-1172, 2006.

23. Lee, H.F., & Yu, H.H. Study of electroactive shape memory polyurethane–carbon nanotube hybrids, *Soft Matter* **7** (8), 3801-3807, 2011.

24. Sun, L., et al. Optimization of the shape memory effect in shape memory polymers, *J. Polym. Sci. Part A: Polym. Chem*. **49** (16), 3574-3581, 2011.

25. Knight, P.T., et al. PLGA-POSS end-linked networks tailored degradation and shape memory behavior, *Macromolecules* **42** (17), 6596–6605, 2009.

26. Weng, S., et al. Shape memory properties of polycaprolactone-based polyurethanes prepared by reactive extrusion, *J. Appl. Polym. Sci.* **127** (1), 748-759, 2012.

27. Zhang, J., et al. Unique multifunctional thermally-induced shape memory poly(p-dioxanone)–poly(tetramethylene oxide)glycol multiblock copolymers based on the synergistic effect of two segments, *J. Phys. Chem. C* **116** (9), 5835-5845, 2012.

28. Xue, L., et al. Synthesis and characterization of three-arm poly(ε-caprolactone)-based poly(ester−urethanes) with shape-memory effect at body temperature, *Macromolecules* **42** (4), 964-972, 2009.

29. Li, F., et al. Shape memory effect of polyethylene/nylon 6 graft copolymers, *Polymer* **39** (26), 6929-6934, 1998.

30. Liu, C., et al. Chemically cross-linked polycyclooctene: synthesis, characterization, and shape memory behavior, *Macromolecules* **35** (27), 9868-9874, 2002.

31. Jeon, H.G., et al. Shape memory and nanostructure in poly (norbornyl-POSS) copolymers, *Polym. Int.* **49** (5), 453-457, 2000.

32. Sakurai, K., et al. Shape-memorizable styrene-butadiene block copolymer. I. thermal and mechanical behaviors and structural change with deformation, *J. Macromol. Sci., Phys. B* **36** (6), 703-716, 1997.

33. Oprea, S. Novel quinoline-based polyurethane elastomers. the effect of the hard segment structure in properties enhancement, *J. Polym. Res.* **19** (1), 9767-9776, 2012.

34. Oertel, G. *Polyurethane Handbook 2*, Hanser, New York, 1993.

35. Pan, M., et al. Morphology and properties of PVC/clay nanocomposites via in situ emulsion polymerization, *J. Appl. Polym. Sci.* **94** (1), 277-286, 2004.

36. Zhu, J., et al. Fire properties of polystyrene-clay nanocomposites, *Chem. Mater*. **13** (10), 3774-3780, 2001.

37. Fornes, T.D., et al. Effect of organoclay structure on nylon 6 nanocomposite morphology and properties, *Polymer* **43** (22), 5915-5933, 2002.

38. Yano, K., et al. Synthesis and properties of polyimide-clay hybrid films, *J. Polym. Sci. Part A: Polym. Chem.* **35** (11), 2289-2294, 1997.

39. Ray, S.S., & Okamoto, M. Polymer/layered silicate nanocomposites: a review from preparation to processing, *Prog. Polym. Sci.* **28** (11), 1539-1641, 2003.

40. Keledi, G., et al. Polymer nanocomposites: structure, interaction, and functionality, *Nanoscale* **4** (6), 1919-1938, 2012.

41. Yoon, J.T., et al. Effects of grafted chain length on mechanical and electrical properties of nanocomposites containing polylactide-grafted carbon nanotubes, *Compos. Sci. Technol*. **70** (5), 776-782, 2010.

42. Bayer, O. *A process for the production of polyurethanes and polyureas*, **German patent DRP 728981**, November 13, 1937.

43. Buehler, W.J., et al. Effect of low-temperature phase changes on the mechanical properties of alloys near composition TiNi, *J. Appl. Phys*. **34** (5), 1475-1477, 1963.

44. Sun, L., et al. Stimulus-responsive shape memory materials: a review, *Mater. Des*. **33**, 577-640, 2012.

45. Spitalsky, Z., et al. Carbon nanotube-polymer composites: chemistry, processing, mechanical and electrical properties, *Prog. Polym. Sci*. **35** (3), 357-401, 2010.

46. Supova, M., et al. Effect of nanofillers dispersion in polymer matrices: a Review, *Sci. Adv. Mater*. **3** (1), 1-5, 2011.

47. Zhou, H., et al. Decoration of Fe_3O_4 nanoparticles on the surface of poly(acrylic acid) functionalized multi-walled carbon nanotubes by covalent bonding, *Polym. Sci. Part A: Polym. Chem.* **48** (21), 4697-4703, 2010.

48. Kong, L., et al. Facile synthesis of multifunctional multiwalled carbon nanotubes/Fe_3O_4 nanoparticles/polyaniline composite nanotubes, *J. Solid State Chem.* **181** (3), 628-636, 2008.

49. Wang, X., et al. Fabrication and characterization of magnetic Fe_3O_4-CNT composites, *J. Phys. Chem. Solids* **71** (4), 673-676, 2010.

50. Zhang, Q., et al. The formation of magnetite nanoparticles on the sidewalls of multi-walled carbon nanotubes, *Compos. Sci. Technol*. **69** (5), 633-638, 2009.

12. S&T benefits accrued:

i. **List of Research publications:**

Sl No.	Authors	Title of the Paper	Name of the Journal	Volume	Pages	Year
1	H. Kalita, N. Karak	Bio-based elastomeric hyperbranched polyurethanes for shape memory application	Iranian Polymer Journal	21	263-271	2012
2	H. Kalita, N. Karak	Mesua ferrea L. seed oil-based hyperbranched shape memory polyurethanes: Effect of multifunctional component	Polymer Engineering and Science	52	2454 – 2461	2012
3	H. Kalita, M Mandal N. Karak	Biodegradable solvent-induced shape-memory hyperbranched polyurethane	Journal of Polymer Research	19	9982 - 9990	2012
4	H. Kalita, N. Karak	Epoxy modified bio-based hyperbranched polyurethane thermosets	Design Monomers and Polymers	16	447-455	2012
5	H. Kalita, N. Karak	Bio-based hyperbranched polyurethane/Fe_3O_4 nanocomposites as shape memory materials	Polymers for Advanced Technologies	24	819–823	2013
6	H. Kalita, N. Karak,	Bio-based hyperbranched polyurethane/multi-walled carbon nanotube nanocomposites as shape memory materials	Polymer Composites	online	DOI: 10.1002/pc.22705	2013
7	H. Kalita, N. Karak	Biobased hyperbranched shape-memory polyurethanes: Effect of different vegetable oils.	Journal of Applied Polymer Science	131	39579	2014
8	H. Kalita, N. Karak	Hyperbranched polyurethane/Fe_3O_4 thermosetting nanocomposites as shape memory materials	Polymer Bulletin	70	2953 - 2965	2013

9	H. Kalita, N. Karak	Hyperbranched polyurethane/triethanolamine functionalized multi-walled carbon nanotube nanocomposites as remote induced smart materials	Polymer International	Online		2013
10	H. Kalita, N. Karak	Fe_3O_4 Nanoparticles Decorated Multi-Walled Carbon Nanotube/Hyperbranched Polyurethane Nanocomposites as Shape Memory Materials	Journal of Nano-engineering and Nano-manufacturing	3	194-201	2013
11	H. Kalita, N. Karak	Bio-based hyperbranched thermosetting polyurethane/triethanolamine functionalized multi-walled carbon nanotube nanocomposites as shape memory materials	Journal of Nanoscience and Technology	Accepted		
12	H. Kalita, N. Karak	Hyperbranched polyurethane /Fe_3O_4 nanoparticles decorated multiwalled carbon nanotube thermosetting nanocomposites as microwave actuated shape memory	Journal of Materials Research	28	2132 - 2141	2013
13	B. Das, N. Karak	Sunflower oil based biodegradable hyperbranched polyurethane as a thin film material	Industrial Crops and Products	44	396–404	2013
14	S. Thakur, N. Karak	Green reduction of graphene oxide by aqueous phytoextracts	Carbon	50	5331 – 5339	2012
15	S. Thakur, N. Karak	Castor oil-based hyperbranched polyurethanes as advanced surface coating materials	Progress in Organic Coatings	76	157–164	2013

16	S. Thakur, N. Karak	Bio-based tough hyperbranched polyurethane–graphene oxide nanocomposites as advanced shape memory materials	RSC Advances	3	9476 - 9482	2013

ii. Manpower trained on the project

a) Research Scientists or Research Associates: Nil

b) No. of Ph. D. produced: 01 (thesis submitted) + 01 (on progress)

c) Other Technical Personnel trained: Nil

iii. Patents taken, if any: No

13. Financial Position:

No	**Financial Position/ Budget Head**	**Funds Sanctioned**	**Expenditure**
I	Salaries/ Manpower costs	₹10,56,000/-	₹ 10,24,744/-
II	Equipment	₹20,00,000/-	₹ 19,06,717/-
III	Supplies & Materials	₹2,58,000/-	₹ 2,55,943/-
IV	Contingencies	₹1,00,000/-	₹ 99,609/-
V	Travel	₹80,000/-	₹ 68,987/-
VI	Overhead Expenses	₹3,00,000/-	₹3,00,000/-
VII	Others, if any		
	Total	**₹37, 94, 000/-**	**₹36, 56, 000/-**

Fund allocated = ₹37,94,000/-

Fund receive = ₹36,56,000/-

Fund utilized = ₹36,56,000/-

14. Procurement/ Usage of Equipment

a)

Sl No.	Name of Equipment	Model/ Make	Cost (FE/ Rs)	Date of Installation	Utilisation Rate (%)	Remarks regarding maintenance/ breakdown
1	Universal Testing Machine	WDW-10, Jinan, China	₹ 19,06,717/-	22/04/2013*	100	Working Satisfactorily

*Only UTM was installed on 22/02/2012, but UTM with Thermal cabinet was installed on 22/04/2013.

b) Plans for utilizing the equipment facilities in future

The equipments shall be utilized for the research work in this university.

Name and Signature with Date

1. Prof. Niranjan Karak
   (Principal Investigator)

2. Prof. Ashok Kumar
   (Co-Investigator)

3. Dr. Manabendra Mondal
   (Co-Investigator)